Accepted Manuscript

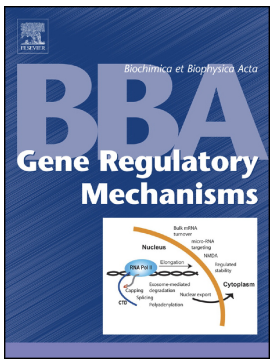

Dicer1 is required for pigment cell and craniofacial development in zebrafish

Andrea M.J. Weiner, Nadia L. Scampoli, Tomás J. Steeman, Christopher M. Dooley, Elisabeth M. Busch-Nentwich, Robert N. Kelsh, Nora B. Calcaterra

PII: S1874-9399(18)30512-1
DOI: https://doi.org/10.1016/j.bbagrm.2019.02.005
Reference: BBAGRM 94362

To appear in: *BBA - Gene Regulatory Mechanisms*

Received date: 25 November 2018
Revised date: 22 February 2019
Accepted date: 23 February 2019

Please cite this article as: A.M.J. Weiner, N.L. Scampoli, T.J. Steeman, et al., Dicer1 is required for pigment cell and craniofacial development in zebrafish, BBA - Gene Regulatory Mechanisms, https://doi.org/10.1016/j.bbagrm.2019.02.005

Dicer1 is required for pigment cell and craniofacial development in zebrafish

Andrea MJ Weiner[1]*, Nadia L Scampoli[1], Tomás J Steeman[1], Christopher M Dooley[2], Elisabeth M. Busch-Nentwich[2,3], Robert N Kelsh[4] and Nora B Calcaterra[1]*

[1] Instituto de Biología Molecular y Celular de Rosario (IBR), Consejo Nacional de Investigaciones Científicas y Técnicas (CONICET) - Facultad de Ciencias Bioquímicas y Farmacéuticas, Universidad Nacional de Rosario (UNR), Ocampo y Esmeralda, (S2000EZP) Rosario, Argentina

[2] Wellcome Trust Sanger Institute, Wellcome Trust Genome Campus, Hinxton CB10 1SA, United Kingdom

[3] Department of Medicine, University of Cambridge, Cambridge, CB2 0QQ, United Kingdom

[4] Department of Biology and Biochemistry, University of Bath, Claverton Down, Bath, United Kingdom

**Corresponding authors:*

Andrea MJ Weiner. IBR (CONICET-UNR) - Ocampo y Esmeralda, (S2000EZP) Rosario, Santa Fe - Argentina. TE: +54-341-423 7070, Ext: 666 - FAX: +54-341-4390465. *E-mail:* weiner@ibr-conicet.gov.ar

Nora B Calcaterra. IBR (CONICET-UNR) - Ocampo y Esmeralda, (S2000EZP) Rosario, Santa Fe - Argentina. TE: +54-341-423 7070, Ext: 655 - FAX: +54-341-4390465. *E-mail:* calcaterra@ibr-conicet.gov.ar

Running title: Dicer1 depletion in developing zebrafish.

Keywords: sox10; neural crest; miRNAs; zebrafish

Abbreviations: microRNA (miRNA); precursor miRNA (pre-miRNA); neural crest (NC); neural crest cells (NCC); hours post-fertilization (hpf); days post-fertilization (dpf); gene regulatory network (GRN); whole mount *in situ* hybridization (WISH)

Abstract

The multidomain RNase III endoribonuclease *DICER* is required for the generation of most functional microRNAs (miRNAs). Loss of *Dicer* affects developmental processes at different levels. Here, we characterized the zebrafish Dicer1 mutant, *dicer1*^{sa9205}, which has a single point mutation induced by N-ethyl-N-nitrosourea mutagenesis. Heterozygous *dicer1*^{sa9205} developed normally, being phenotypically indistinguishable from wild-type siblings. Homozygous *dicer1*^{sa9205} mutants display smaller eyes, abnormal craniofacial development and aberrant pigmentation. Reduced numbers of both iridophores and melanocytes were observed in the head and ventral trunk of *dicer1*^{sa9205} homozygotes; the effect on melanocytes was stronger and detectable earlier in development. The expression of *microphthalmia-associated transcription factor a* (*mitfa*), the master gene for melanocytes differentiation, was enhanced in *dicer1*-depleted fish. Similarly, the expression of *SRY-box containing gene 10* (*sox10*), required for *mitfa* activation, was higher in mutants than in wild types. *In silico* and *in vivo* analyses of either *sox10* or *mitfa* 3'UTRs revealed conserved potential miRNA binding sites likely involved in the post-transcriptional regulation of both genes. Based on these findings, we propose that *dicer1* participates in the gene regulatory network

governing zebrafish melanocyte differentiation by controlling the expression of *mitfa* and *sox10*.

1. Introduction

Fundamental biological processes such as embryonic development, cell differentiation, growth, death, and cancer are regulated by microRNAs (miRNAs) [1,2]. miRNAs are evolutionally conserved endogenous noncoding small RNAs (~22 nucleotides in length) able to regulate gene expression at the posttranscriptional level [3]. In general, miRNAs are transcribed by RNA polymerase II yielding primary transcripts that are processed to precursor miRNA (pre-miRNA) by the ribonuclease Drosha in the nucleus. Pre-miRNA is exported to the cytoplasm where the ribonuclease Dicer produces a short double-stranded RNA (20 to 25 nucleotides). Dicer facilitates the activation of the RNA-induced silencing complex, which is essential for miRNA functional maturation [4]. Therefore, Dicer is required for generation of most functional miRNAs.

In mice, *Dicer* deletion causes the loss of the inner cell mass of the blastocyst resulting in early embryonic lethality [5]. However, in zebrafish, homozygous *dicer1*$^{-/-}$ mutants undergo growth arrest at 8 days post fertilization (dpf) and die at 14–15 dpf [6,7]. Inhibition of *dicer1* mRNA translation by injection of antisense morpholino oligonucleotides (Dicer1-MO) in wild-type embryos produces a more severe phenotype, consistent with a contribution of maternal Dicer1 to early development [6]. The zebrafish maternal-zygotic Dicer1 mutant (*MZdicer*) shows the most severe phenotype; embryos display defective gastrulation resulting in a reduced extension of

the axis, as well as impaired brain, somite, heart, and ear development [8]. Most of these defects are rescued by the injection of members of the miR-430 family. miR-430 plays key roles in the clearance of maternal mRNAs shortly after the activation of the zygotic genome [9,10] thus ensuring proper transitions between different developmental stages [11].

The neural crest (NC) is a transient, multipotent stem cell-like population whose formation occurs early in development at the border of the developing neural tube. After closure of the neural tube, NC cells (NCC) experience an epithelial-to-mesenchymal transition in order to delaminate and migrate away, undergoing some of the longest distance migrations of any embryonic cell type [12]. NCC differentiate into a variety of derivatives, including neurons and glia of the enteric, sensory, and autonomic nervous system, pigment cells of skin, chromaffin cells, bone and cartilage of the face, endocrine cells, cardiac structures, smooth muscle cells, and tendons [13]. Different gene regulatory networks (GRN) control the specification, delamination, migration, and differentiation of NC cell type [14]. Specific deletion of *Dicer* in mouse NCC results in increased apoptosis of differentiating cells, but did not prevent initial differentiation of craniofacial and peripheral nervous system derivatives [15–18]. Although it is known that miRNAs play important roles in the GRN of NC development, posttranscriptional regulation by miRNAs has not been deeply characterized yet [19,20]. In mice, the expression of *Mitf* (*microphtalmia-associated transcription factor*), the key master gene for melanocyte specification [21,22], is directly regulated by a set of miRNAs [23–25]. As Mitf activates *Dicer* transcription, the existence of a feedback loop between Mitf and Dicer during mammalian melanocyte differentiation has been suggested [25,26]. In zebrafish, *sox10* expression is required for the

transcriptional activation of *mitfa* (the *Mitf* orthologue) and the specification of the melanocyte lineage [27]. However, as Sox10 represses the expression of melanogenic enzyme genes, its expression has to be repressed for melanocyte differentiation progression [28].

Here we generated and characterized a novel zebrafish *dicer1* mutant line. Our results show that *dicer1*-depletion in zebrafish affects craniofacial development and pigmentation likely by impairing the generation of mature miRNAs involved in the post-transcriptional regulation of *sox10* and *mitfa* during NC development.

2. Materials and Methods

2.1 Ethics statement for animal care

All embryos were handled according to relevant national and international guidelines. All procedures using zebrafish from the Calcaterra lab were authorized by the Comité Institucional para el Cuidado y Uso de Animales de Laboratorio of the Facultad de Cs. Bioquímicas y Farmacéuticas-Universidad Nacional de Rosario, which has been accepted by the Ministerio de Salud de la Nación Argentina (http://www.saludinvestiga.org.ar/comites.asp?num_prov=13); files N° 6060/296 and 351/2016. Animals in the Kelsh lab are housed in a facility certified by the Home Office, and the work was approved by the University of Bath Animal Welfare and Ethical Review Body and performed under Home Office Project Licenses PPL30/2415 and PPL30/2937. Zebrafish at the Wellcome Trust Sanger Institute were maintained in accordance with UK Home Office regulations, UK Animals (Scientific Procedures) Act

1986, under project licence 70/7606, which was reviewed by the Wellcome Trust Sanger Institute Ethical Review Committee.

2.2 Animal handling and microinjection of zebrafish embryos

Adult zebrafish were maintained at 28°C on a 14:10 h light:dark cycle as previously described [29]. Wild-type matings usually involved crossing three males and four females in the same spawning tank. For mutants or transgenic embryos, one female and one male were set up in crossing tanks. All embryos were staged according to morphological development in hours or days post-fertilization (hpf or dpf, respectively) at 28°C [30]. Embryos were injected at one-cell stage into the yolk immediately below the cell using a gas-driven microinjection apparatus (MPPI-2 Pressure Injector, Applied scientific Instrumentation; Eugene, OR, USA).

2.3 Adult caudal fin and embryo DNA genotyping

DNA samples were obtained from 30 hpf embryos or adult tails as previously described [29]. Genomic region for *dicer1* point mutation was amplified by PCR using the specific oligonucleotides: gMutDicer1For: TTAAGGAGGCAGGAAAGCAA, gMutDicer1Rev: TTCATGGGCTCTGAATTTCC, purified and sequenced by DNA Sequencing Facility of University of Maine, USA. Results were compared to zebrafish genome using the Blat tool of UCSC Genome Browser [31].

2.4 Antisense morpholinos

Morpholinos were acquired from Gene Tools (Philomath, OR, USA), with the sequences as follow, Dicer1-MO: 5'- CTGTAGGCCAGCCATGCTTAGAGAC; mismatch

control Dicer1-mmMO contains four mismatches (underlined in the sequence): 5'-CTCTAGGCCTGCCATCCTTAGTGAC. Morpholinos were injected as described elsewhere [6].

2.5 Alcian blue staining

Four dpf larvae were fixed in 4% (w/v) paraformaldehyde (PFA) in phosphate-buffered saline 1X (PBS) with 0.1% (v/v) Tween-20 (PBT 1X), and washed in PBT 1X four times. The protocol was performed as detailed elsewhere [32]. Pictures of cartilage staining larvae were taken with a BH2 Olympus Microscope and Nikon DS-Fi1 digital camera. Cranial cartilages measurements were done as reported elsewhere [33,34], by using the ImageJ software (National Institutes of Health, Bethesda, MD, USA) [35].

2.6 Melanin quantification and black pigment cell counting.

Thirty embryos of 28 and 48 hpf were manually dechorionated and used to measure melanin levels as previously described [36]. Results were obtained and processed from five independent experiments for each condition. For melanocyte counts, ten larvae of each condition were treated with epinephrine to contract melanosomas, as described elsewhere [37]. Results from three independent pools of larvae were included. In the Tg(*sox10*:GFP) line, green fluorescence was examined at each time point in at least 20 pigmented cells from each of 5 fish (i.e. n = 100).

2.7 Acridine Orange apoptosis analysis

Live wild-type or Tg(*sox10*:mRFP) [38] embryos were injected with Dicer1-MO or Dicer1-mmMO and manually dechorionated. At corresponding stages, embryos were

stained with the vital dye Acridine Orange as previously described [39]. Injections and staining were repeated four independent times. Fluorescence in embryos was analyzed under a dissecting Microscope Olympus MVX10 and an inverted Microscope Olympus IMT2. Pictures were taken with either a BH2 Olympus Microscope and a Nikon DS-Fi1 digital camera or a Zeiss LSM 880 confocal laser-scanning Microscope.

2.8 mRNA whole-mount in situ hybridization

Embryos were staged and fixed overnight in 4% (w/v) PFA in PBS 1X at 4°C. After washing, embryos were stored in methanol at -20°C until their use. The procedure for whole-mount *in situ* hybridizations (WISH) was carried out as previously described [40]. Digoxigenin-uracil triphosphate-labeled riboprobes were prepared according to the manufacturer's instructions (Roche Diagnostics, Mannheim, Germany). Microscopic examination was performed with a BH2 Olympus Microscope and a Nikon DS-Fi1 digital camera.

2.9 Plasmid constructs

Zebrafish *sox10* and *mitfa* 3'UTR sequences were amplified from late embryonic stage cDNA preparations using specific primers with *Xho*I sites (marked in lowercase; 3'UTRsox10F: CCGctcgagACACTCTACCAAGATGACCAGT, 3'UTRsox10R: GGCctcgagTGCAGCTTTATTTAGAGTGAGGA, 3'UTRmitfaF: CCGctcgagTGCCAACTAAATTTCATGAACCA, and 3'UTRmitfaR: GGCctcgagAGCTACTCTTTATATCATCCGCG). PCR amplified products were cloned in pGEM-T Easy Vector System (Promega) and sent to sequence as described above in section 2.3. Plasmid preparations from positive clones were purified and cut at their

ends with *Xho*I restriction enzyme (Thermo Scientific) for sub-cloning in *Xho*I site downstream of EGFP in pCS2+MT vector system. Sub-cloning of *sox10* 3'UTR-F0 region was performed using previously described forward oligonucleotide (3'UTRsox10F) with specific reverse oligonucleotide (3'UTRsox10-F0_R: TGCtctagaTGCAGATCTCCACACACACA), cutting with *Xho*I and *Xba*I restriction enzymes. Sub-cloning of *sox10* 3'UTR-F2 region was performed using specific forward oligonucleotide (3'UTR-sox10-F2_F: CCGctcgagCGCCATACACACATGTCTCC) with previously described reverse oligonucleotide (3'UTRsox10R), cutting with *Xho*I restriction enzyme. Since 3'UTR-*sox10* has an internal *Xba*I restriction site at 650 bp, 3'UTR-*sox10*-F1 region was sub-cloned from the full-length version of 3'UTR-*sox10* in pCS2+MT plasmid and cut with *Xba*I restriction enzyme, purified and ligated. Selected plasmids were enzyme digested and/or sequenced to obtain the ones with the correct 3'UTR orientation, cut with *Not*I restriction enzyme (Thermo Scientific) to be templates for *in vitro* mRNA transcription using mMESSAGE mMACHINE® SP6 Transcription Kit (Ambion) following the manufacturer instructions. Five nl of 100 ng/µl dilution of each mRNA were microinjected. EGFP expression was initially observed in live embryos using a fluorescent dissecting Microscope Olympus MVX10.

2.10 RT-qPCR assays

Total RNA from 40 embryos was obtained using TRIZOL® Reagent (Invitrogen) following the manufacturer's instructions. Purified RNA was incubated with RQ1 DNAse (Promega) and retro-transcribed with Revert Aid RT enzyme (Thermo Scientific) using oligo(dT) primer. Quantitative PCR (qPCR) reactions were performed using four different RNA purifications and three independent experiments using an Eppendorf

Realplex4 and standard temperature protocol. Primer sequences were as follows: *bcl2l11* forward, GATGAACCGGACTTTCTCCA; *bcl2l11* reverse, TGCTGGTGGCTATGTTCTGA; *dct* forward, TCTTCCCACCTGTGACCAAT; *dct* reverse, ACATAGCCGGTCTGTTGTCC; *dicer1* forward, ATCGCTAGCTGGTGCAATTT; *dicer1* reverse, GTCTCTGGCTCCATCTCCAG; *egfp* forward, TTCAGCCGCTACCCCGACCA; *egfp* reverse, ACCAGGGTGTCGCCCTCGAA; *mitfa* forward, CTGGACCATGTGGCAAGTTT; *mitfa* reverse, TGAGGTTGTGGTTGTCCTTCT; *sox10* forward, AAAACACTGGGGAAGCTGTG; *sox10* reverse, ACGTGGCTGGTACTTGTACT; *tyr* forward, ACTTCATGGTGCCCTTCATC; *tyr* reverse, CAGGAACTCCTGCACAAACC; *tyrp1b* forward, CGACAACCTGGGATACACCT; *tyrp1b* reverse, TACAACCAGCACCACTGCAA. Predicted PCR products span at least one intron, to ensure amplification solely from the cDNA and not from genomic DNA, except for *egfp*. *Ef1α* and *rpl13* were used as endogenous control for normalization analysis [41]. Data were analyzed using qBase software version 2.2 and t-student tests were employed as indicated. The validity of the RT-qPCR data was assured by following the MIQE guidelines [42].

2.11 Western blotting

Fifty embryos staged at 26 hpf were dechorionated and processed as reported elsewhere [33]. Rabbit polyclonal anti-actin (I-19; sc-1616-R) was from Santa Cruz Biotechnology, while Rabbit polyclonal anti-GFP (ab290) was from Abcam (Cambridge, UK). Membranes were incubated with the appropriate primary and HRP-conjugated antibodies (1/7000 to 1/25000 dilution), washed and developed using chemiluminescence (SuperSignal West Pico Chemiluminescent Substrate, Thermo

Fisher Scientific) and X-ray films (Amersham Hyperfilm ECL, GE Healthcare Science, Chicago, IL, USA). Relative protein concentrations were determined as reported [33].

3. Results

3.1. The zebrafish dicer1^{sa9205} mutant line displays abnormal development.

The zebrafish *dicer1^{sa9205}* mutant line was generated by the Zebrafish Mutation Project at the Wellcome Trust Sanger Institute [43,44]. A single point mutation changing a cytosine to adenine (C>A) in exon 9 is predicted to generate a truncated protein of 459 amino acids, which lacks all conserved motifs except the DEAD-box motif (Figure 1A). Heterozygous *dicer1^{sa9205}* developed normally, being phenotypically indistinguishable from wild-type siblings; embryos were raised to adulthood, genotyped for the point mutation, and crossed to generate homozygous mutants. In homozygous *dicer1^{sa9205}* mutants, initial development appeared morphologically normal up to 48 hpf. Thereafter, smaller eyes, similar to the phenotype reported in *Dicer1* mutant mice [45] and fish [7], as well as defects in head and brain began to be observed (Figure 1F-G). Phenotypic differences were also distinguishable at 72 hpf (Figure 1H-I). Most of the homozygous *dicer1^{sa9205}* larvae died by 10 dpf, and no *dicer1^{sa9205}* fish survived beyond two weeks of development. Similar phenotypes were previously reported for three different *dicer1* mutant alleles [6]. To confirm that this phenotype results from homozygosis of the *dicer1^{sa9205}* allele, a series of test crosses were performed in order to assay the Mendelian inheritance pattern of the mutant phenotype (Supplementary Figure 1A). The described mutant phenotype was only obtained when crossing *dicer1^{sa9205}* heterozygous mutants; in these crosses, the ratio

of wild-type:mutant phenotypes was indistinguishable from the expected 3:1 ratio (Chi-squared test; p=0.9999). Mutant embryos were genotyped in order to associate *dicer1*^{sa9205} point-mutation with phenotype (Supplementary Figure 1B).

A *dicer1*-specific morpholino (Dicer1-MO; Supplementary Figure 2) and a mismatch control morpholino (Dicer1-mmMO) were used as previously reported by Wienholds et al. [6] to further test the consequences of Dicer1 depletion on zebrafish embryonic development. Morphological malformations in *dicer1*-morphants were similar to, but exaggerated compared with, those observed in *dicer1*^{sa9205} mutants (Supplementary Figure 2).

3.2. Effects of dicer1 depletion in neural crest derivatives.

Defects in craniofacial development were clearly detected when larvae from a *dicer1*^{sa9205} heterozygote incross were fixed at 96 hpf and stained with Alcian Blue (Figure 2). Dicer1-depletion caused significant shortening of Meckel (M), ceratohyal (CH) and hyosymplectic-palatoquadrate (PQ) cartilages lengths (Figure 2A, N=32). The Meckel area (defined as the area of triangle shaped by Meckel cartilages; Fig. 2A), the distance between ceratohyal cartilages joint and the lateral fins, and the cranial distance (measured as the distance from the anterior-most M to the lateral fins) also showed significant reductions (Figure 2A, N=32; compare C with D). The reductions observed in mutants affected the normal extension of the lower mandible (Meckel cartilage) beyond the upper one (ethmoid plate; see arrowheads in Figure 2C and D). Moreover, the angle formed by the ceratohyal cartilages was significantly more acute than in controls (Figure 2B, N=32; compare C with D). In the case of *dicer1*-morphants, more severe phenotypes were detected (Figure 2E). Our results are consistent with

previous data gathered in *dicer* mutant mice [15–18], suggesting conservation of the role for Dicer1 in craniofacial development.

Pigmentation was also affected in *dicer1*^{sa9205} mutants and *dicer1*-morphants. Zebrafish pigmentation is characterized by the presence of melanocytes, iridophores, and xanthophores, three different kinds of pigment cells derived from NCC [46].

Iridophores produce the iridescent pigment on the eyes, on top of the head, scattered amongst melanocytes in the body and in discrete 'lateral patches' above the yolk sac in the anterior trunk, as seen in 72 hpf control larvae (Figure 3A-B). We found a decrease in the extent of iridophores on the eye and in the lateral patches of *dicer1*^{sa9205} homozygotes and *dicer1*-morphants (Figure 3C-F).

Melanocytes showing the black pigment melanin are evident by 25 hpf in zebrafish embryos, initiating in the region just posterior to the otic vesicle [46]. At 28 hpf, *dicer1*^{sa9205} mutants showed reduced number of pigmented melanocytes, especially in the posterior hindbrain region (compare the zone marked by the red arc in Figures 1B' and D'). Differences were still detectable in the hindbrain region at 32 hpf (compare the zone outlined by the red oval in Figures 1C' and E'). By 48 hpf, mutants displayed a decreased number of melanocytes, as well as decreased melanin (visible as greyer, less black, coloration) in remaining melanocytes, compared to wild-type siblings (Figure 1F-F' and G-G'). At 72 hpf, differences in the melanin intensity and the number of melanocytes located in the head, lateral stripe, and yolk were observed in mutant larvae (Figure 1H-H', I-I', and Figure 3A-D). Similar phenotypic defects in melanocyte differentiation were observed for *dicer1*-morphants (Supplementary Figure 2). Importantly, black pigmentation of the pigmented retinal epithelium (melanocytes here are derived from the brain, and not from the NC) was unaffected in both

dicer1^{sa9205} mutants and *dicer1*-morphants (Figure 1 and Supplementary Figure 2), suggesting a specific effect of Dicer1 depletion on pigment cells derived from the NC.

To assess NCC development when Dicer1 was depleted, we used the Tg(*sox10*:GFP) zebrafish line [47] that expresses the fluorescent protein under the control of the *sox10* promoter. Transgenic embryos injected with *dicer1*-MO and examined at 38 hpf displayed increased numbers of GFP-labeled xantophores, which may be due to a difference in the timing since their morphology and patterning appears to be normal (Figure 3G-L). To assess melanocyte development, we examined GFP fluorescence in cells displaying melanin, assessing the rate of GFP quenching due to melanin accumulation [28]. Melanised cells in the posterior trunk were selected randomly with respect to dorso-ventral position, and scored for detectable GFP. In Dicer1-mmMO specimens staged at 30 hpf, almost all melanocytes showed detectable GFP expression, but green fluorescence rapidly decreased by 54-57 hpf, comparable to published observations in wild-types [28]. In contrast, *dicer1*-morphants at the same developmental stages contained significantly higher percentages of dark cells expressing GFP (Figure 3M). Results reinforce the notion that the synthesis of melanin is affected in *Dicer1*-depleted specimens.

To address the mechanisms underlying the observed phenotypes, we measured the level of melanin in *dicer1*-morphants and *dicer1*^{sa9205} mutants at different developmental stages, following an established protocol [36]. Both *dicer1*-morphants and *dicer1*^{sa9205} mutants showed significantly decreased levels of melanin when compared to 48 hpf-staged controls, whereas differences in melanin levels between morphants and mutants were undetectable (Figure 3N).

3.3 Dicer1 depletion induces apoptosis of melanocyte precursors

As noted above, *dicer1*-depleted fish show an apparent decrease in the number of melanocytes. To determine the impact of Dicer1 depletion on the number of melanocytes, we incubated zebrafish larvae with epinephrine to contract melanosomas [37] and fixed them at different developmental stages. A significant lowering in the number of melanised cells in the head (Figure 4A) and in the lateral stripe alongside the yolk sac extension (Figure 4B) of *dicer1* depleted zebrafish was observed. The reduction in the number of melanised cells could represent the extreme of reduced melanin (i.e. melanocyte is there but has too little melanin to see it), or could reflect another mechanism (defect in specification/survival/proliferation) causing absence of some melanocytes.

In mouse, Dicer knockdown results in significant loss of NC derivatives by apoptosis, with reduced proliferation not observed [15]. Therefore, we used Acridine Orange staining of apoptotic cells to assess *in vivo* cell death in *dicer1*^{sa9205} mutants and *dicer1*-morphants. At 28 hpf, *dicer1*^{sa9205} mutants and *dicer1*-morphants displayed levels of apoptosis in the cephalic region significantly higher than controls (n= 50; Figure 5A). In order to establish if a subset of these apoptotic cells belong to the NC lineage, we performed Acridine Orange staining on Tg(*sox10*:mRFP) embryos in which NCC are labeled with membrane-tethered RFP [38]. Confocal microscopy of both 26 hpf (Figure 5E' and E") and 32 hpf (Figure 5H' and J') *dicer1*-depleted embryos revealed higher numbers of green or yellow fluorescent nuclei (Acridine orange labeling; white arrowheads) in NCC, compared to controls (Figure 5D', G' and I'). Dying melanised cells were not detected in *dicer1*-morphant specimens at 42 and 48 hpf (n= 50; not shown). These results suggest that a group of NCC, likely including melanocyte precursors, die

by apoptosis when Dicer1 is depleted. The otic vesicles express *sox10*, but are not NC-derived. Interestingly, we did not detect any apoptotic nuclei in the otic vesicle cells of either morphants nor in controls (Figure 5K' and L'), suggesting a level of specificity to the apoptosis seen in the NC.

In human cells, the pro-apoptotic factor BIM has been shown to play a critical role in melanocyte survival and to be a target of the miRNA-17~92 cluster [25]. Through *in silico* studies, we detected three putative binding sites for miRNA-17 family in the 3'UTR of *bcl2l11*, the zebrafish orthologous BIM factor (Targetscan: www.targetscan.org, not shown). As expected, the expression of *bcl2l11* measured by RT-qPCR in both *dicer1*^{sa9205} mutants and *dicer1*-morphants was significantly higher than in controls (Figure 5B). These data indicate that, similar to in human cells, Dicer1 depletion in zebrafish embryos leads to increased apoptosis of NCC, likely due to mis-regulation of the pro-apoptotic factor *bcl2l11*.

3.4 Mitfa regulates dicer1 expression during zebrafish development

Mitf is usually considered the master regulator controlling melanocyte differentiation, through Mitf-binding to E-boxes in the promoter regions of numerous target genes, including *dopachrome tautomerase* (*dct*), *tyrosinase* (*tyr*), *tyrosinase-related protein 1* (*tyrp1*), *silver* (*si*), and *sox10* [28,48]. Studies performed with human primary melanocytes showed that *DICER* is a *MITF* target [25]. MITF acts as a direct regulator of *DICER* through two CA(CA/TG)TG conserved consensus binding sites identified in the human and mouse promoters [25]. We hypothesized that a similar regulatory relationship exists in zebrafish. *In silico* analysis of the *dicer1* promoter region (defined as 3000 bp upstream of the transcription start site) revealed thirteen

putative E-boxes, one of them displaying the conserved CATGTG consensus binding site sequence (Figure 6A). We then tested *dicer1* expression at different developmental stages in the zebrafish *mitfa*$^{w2/w2}$ mutant line [22] by RT-qPCR and observed a transient reduction in the levels of *dicer1* expression in 30 to 36 hpf *mitfa*$^{w2/w2}$ embryos compared with wild type siblings (Figure 6B). Later in development, the level of *dicer1* did not differ from that measured in wild-type larvae. These data are consistent with the suggestion that the MITF-DICER regulatory feedback loop found in humans may also function in zebrafish.

3.5 Dicer1 depletion enhances the expression of mitfa and sox10

Experiments performed in zebrafish combined with an iterative mathematical modeling approach established a core GRN for melanocyte differentiation [28]. This model shed light on the relation between transcription factors and regulation of their expression, identifying multiple regulatory loops controlling the progression of melanocyte differentiation. In particular, a feed forward-repression loop was shown to control *sox10* expression. Several groups have shown that Sox10 can directly activate Mitf expression [27,49,50], while in fish prevent the expression of melanogenic enzyme genes [28]. In zebrafish, a decrease in *sox10* mRNA levels from 28 hpf onwards was observed, and their modeling studies suggested this might function to allow the expression of melanogenic enzyme genes [28]. These observations led us to evaluate by RT-qPCR and whole mount *in situ* hybridization (WISH) assays the expression of *sox10* and *mitfa* in Dicer1-depleted zebrafish specimens. The relative amount of *sox10* mRNA was significantly enhanced in both *dicer1*^{sa9205} and *dicer1*-morphants at all stages analyzed (from 28 to 48 hpf; Figure 7A), and *mitfa* mRNA levels were

significantly enhanced in *dicer1*^{sa9205} (28 and 48 hpf) and *dicer1*-morphants (from 28 to 48 hpf; Figure 7B). A consistent expansion of the *sox10*-expression territory in the cranial ganglia, and trunk NCC was often detected by WISH in mutants (Figure 7C, D, G, and H, labeled with white ovals and rectangles; 31/40). Similar observations were obtained in *dicer1*-morphants for *sox10* and *mitfa* expression patterns (not shown). *Dicer1*-depleted embryos consistently showed this aberrant pattern with overexpression at 28 hpf. WISH is at best semi-quantitative, so it is perhaps not surprising that we were unable to detect a change in expression levels of *mitfa* in the mutants. Nevertheless, our data indicate that Dicer1 depletion causes an increase in the relative abundance of *sox10* and *mitfa* mRNAs.

3.6 Dicer1 depletion affects the expression of tyrosinase.

In mice, melanin biosynthesis is mediated by a group of enzymes uniquely expressed in melanocytes, called the tyrosinase-related protein (TRP) family, composed of tyrosinase (Tyr), Tyrp1 (originally termed TRP1), and Dct (originally termed TRP2) [51–53]. Tyr is the critical and rate-limiting enzyme required for melanogenesis, catalyzing the initial reaction of tyrosine hydroxylation. Tyrp1 and Dct have distinct catalytic functions in melanin synthesis downstream of Tyr. In contrast to mutations in Tyr, mutations in Tyrp1 or Dct affect the quality of melanin synthesized rather than the quantity [54,55]. The expression of *dct*, *tyr*, and *tyrp1b* genes was assessed in *dicer1*^{sa9205} and *dicer1*-morphant embryos staged between 28 and 48 hpf. RT-qPCR measurements revealed no significant changes in the relative amounts of *dct* and *tyrp1b* transcripts in *dicer1*^{sa9205} and *dicer1*-morphants (Figure 7O and Q). However, a significant reduction in the expression of *tyr* mRNA was detected in both

dicer1^{sa9205} and *dicer1*-morphants (36 and 48 hpf; Figure 7P). Conversely, changes in mRNA levels of either of the studied genes were barely detected by WISH (Figure S3). Similar observations were obtained in *dicer1*-morphants for all tested genes (not shown). Differences measured by RT-qPCR were not detected by WISH perhaps due to the semi-quantitative nature of this technique. Nevertheless, results suggest that the pale phenotype of *dicer1*^{sa9205} mutants could be partially due to *tyr* down-regulation. Bearing in mind the GRN suggested by Greenhill and colleagues [28], it is tempting to speculate that *tyr* downregulation results from *sox10* up-regulation due to Dicer1 depletion. The fact that *tyrp1b* expression has not been affected by Dicer1-depletion is consistent with this hypothesis, since Greenhill et al. [28], showed that *tyrp1b* regulation is not controlled by *sox10*.

3.7 The expression of sox10 and mitfa can be regulated at the 3'UTR level

The up-regulation of *sox10* and *mitfa* as a consequence of *dicer1* depletion suggests a role for miRNAs in the posttranscriptional regulation of both genes. To test this, we searched for the presence of conserved putative miRNA binding sites located in the *sox10* and *mitfa* 3'UTR by using the TargetScan program. Eleven conserved miRNA binding sites were found in the *sox10*-3'UTR and five in the *mitfa*-3'UTR (Figure 8A-B). Both the *sox10*-3'UTR and *mitfa*-3'UTR sequences were cloned downstream of an EGFP coding sequence, as described in Materials and Methods. Constructs were used to synthesize *in vitro* the corresponding *EGFP*-mRNA-*sox10*-3'UTR (*sox10*-3'UTR) and *EGFP*-mRNA-*mitfa*-3'UTR (*mitfa*-3'UTR) mRNAs. An *EGFP*-mRNA (SV40-poly(A)) was synthesized in a similar fashion and used as a control. mRNAs were purified and injected in one-cell zebrafish embryos. EGFP-positive embryos at 50% of epiboly were

allowed to develop until 24 hpf when EGFP protein expression levels were assessed by Western blot assays (Figure 8C). A significant reduction of EGFP protein was detected on embryonic extracts prepared from *EGFP-mRNA-sox10-3'UTR* or *EGFP-mRNA-mitfa-3'UTR* injected embryos (Figure 8D). Next, EGFP-positive embryos were collected at 24 or 30 hpf stages for total RNA extraction. RT-qPCR showed a significant temporal reduction in the level of both *sox10-3'UTR* and *mitfa-3'UTR* but not in *EGFP*-mRNA (Figure 8E). Then, we evaluated at 24 hpf the relative amount of *EGFP-mRNA* when *EGFP-mRNA-sox10-3'UTR* and *EGFP-mRNA-mitfa-3'UTR* were co-injected with Dicer1-mmMO or Dicer1-MO. With Dicer1-mmMO, the presence of either the *sox10* or *mitfa* 3'UTR sequences led to a reduction in the *EGFP*-mRNA. However, the co-injection of mRNAs with Dicer1-MO fully recovered the levels of transcript (Figure 8F). Finally, we decided to make three different versions of *sox10*-3'UTR in order to detect a minimal region that is controlled by miRNA regulation. F0 fragment does not have any predicted miRNA-binding site, F1 fragment has four miRNA target sites, and F2 fragment contains seven miRNA target sites (Figure 8A). The analysis of these three fragments was performed as previously described (Figure 8C), and total RNA extracts were prepared from embryos at 24 hpf. The relative amount of *EGFP-mRNA* was evaluated when *EGFP-mRNA*-F0-*sox10-3'UTR, EGFP-mRNA*-F1-*sox10-3'UTR,* and *EGFP-mRNA*-F2-*sox10-3'UTR* were co-injected with Dicer1-mmMO or Dicer1-MO. For F0 fragment, no differences were detected when injected with either MO (Figure 8G), indicating that this fragment is not regulated by miRNAs. With Dicer1-mmMO, the presence of either the F1 or F2 fragments led to a reduction in the *EGFP*-mRNA. Conversely, the co-injection of mRNAs with Dicer1-MO only fully recovered the levels of transcript for F1 fragment. Similar results were obtained when co-injecting F1+F2

fragments and MOs (data not shown). Although an artificial *EGFP*-mRNA decay due to the fact that the F2 fragment was analyzed out of the endogenous context cannot be ruled out, results suggest that the F1 fragment contains elements potentially involved in miRNAs-mediated regulation of *sox10* expression. Our data suggest that, at developmental stages wherein melanocyte differentiation is taking place, *sox10* and *mitfa* are post-transcriptionally regulated by miRNAs (Figure 8H).

4. Discussion

Dicer is required for the production of small RNA molecules that regulate gene expression, playing a critical role in early embryonic development. While Dicer knock-out mice die at blastocyst stage [5], zebrafish Dicer1 mutant fish are not embryonic lethal and go through early developmental stages, likely due to the function of maternal Dicer1 [56]. This is supported by the observation that Dicer1-MO caused an earlier developmental arrest and a more severe phenotype [56], and that depletion of both maternal and zygotic zebrafish Dicer1 resulted in an even earlier embryonic phenotype, affecting gastrulation and somitogenesis [8]. NC development was noticeably affected in *dicer1*^{sa9205} mutant fish, as revealed by craniofacial (Figure 2) and pigment cell defects (Figures 1, 3, and 4). Craniofacial defects have been previously reported in Dicer mutant mice specific for NCC [15–18]. Craniofacial defects may be a consequence of aberrant ribosome biogenesis, since Dicer is important for nucleolar pre-rRNA processing [57] and it associates with rDNA [58]. Of note, effects on pigment cells have not been reported yet. Based on a combination of genetic experimentation and mathematical modeling, the GRN associated with melanocyte specification and differentiation has been considerably expanded and refined in

embryonic zebrafish [28]. Here, we explored the hypothesis that the melanocyte GRN can be modulated through the activity of Dicer1 and miRNAs for the proper cell specification and differentiation. In particular, we gathered data suggesting that Dicer1 and miRNAs are involved in the fine-tuning of *mitfa* and *sox10* expression, likely by controlling the feed-forward loop between both transcription factors (Figure 8H).

It has been reported that Mitf regulates Dicer expression at the transcriptional level in human cell culture. *In silico* evaluation of the zebrafish *dicer1* promoter region reveals several putative E-boxes, and lower levels of *dicer1* transcripts were detected in a homozygous *mitfa* mutant background. It seems that Mitf is required for proper *dicer1* transcription not only in mammals [25] but also in fish; thereby, this requirement may be ancestral. Developmental stages where *dicer1* down-regulation was observed in *mitfa* mutants (30-36 hpf) overlap with both the highest expression level reached by *mitfa* and the start point of *sox10* mRNA down-regulation in wild types [28]. Our results suggest that *sox10* down-regulation is temporally correlated with Mitf-dependent expression of *dicer1* and subsequent production of miRNAs in melanocytes.

Several mechanisms may contribute to the abnormal development of melanocytes in Dicer1-depleted embryos. Results from Acridine Orange assays showed increased apoptotic nuclei in NCC of Dicer1-depleted embryos. This finding agrees with data gathered in Dicer-knockout mutant mice, wherein loss of both melanocyte stem cells and differentiated melanocytes was observed by TUNEL [25]. In mice, Dicer depletion prevents the processing of the pre-miRNA-17~92, leading to the overexpression of BIM, a known pro-apoptotic regulator of melanocyte survival [25]. In a similar fashion, the relative amount of *bcl2l11* mRNA was higher in *dicer1*-depleted zebrafish embryos,

suggesting the possibility of a conserved mechanism involving DICER in cell survival during vertebrate melanocyte differentiation. Thus, the levels of *bcl2l11* may play a significant role in lineage survival, although it is probable that other miRNAs than miR-17~19 cluster as well as apoptotic regulators could contribute to control melanocytic survival. Further work to assess the cell autonomy of melanoblast death and of *bcl2l11* up-regulation in these cells will be important to test this suggestion.

Apart from the role of Dicer and miRNAs in melanocyte precursor survival, Dicer1 depletion may also hamper melanocyte differentiation by affecting the expression of genes of the GRN. Indeed, when Dicer1 was lowered, *mitfa* expression was increased. In addition, our *in vivo* assay showed that the presence of *mitfa* 3'UTR affects the amount of EGFP either at mRNA or protein levels in a Dicer1-dependent manner, and suggests that Mitfa expression is regulated by miRNAs. Several studies have already reported a link between the *mitfa* 3'UTR and miRNAs [23,59,60]. Therefore, miRNA-dependent regulation of *mitfa* expression may be conserved in zebrafish melanocyte development. The novelty of our work lies in the finding that *sox10* expression may also be controlled by miRNAs in the GRN governing melanocyte differentiation. When *dicer1* was lowered by Dicer1-MO injection or in *dicer1*^{sa9205} mutants, *sox10* transcript levels were higher. Besides, the normal decay of *sox10* expression during melanocyte differentiation was perturbed in Dicer1-MO treated embryos. We were able to delimit a region of the *sox10* 3'UTR likely responsible for miRNA regulation, thus opening new opportunities to address questions regarding the role of miRNAs in NCC differentiation during embryonic development. Further research in our laboratory will target a better understanding of the mechanisms underlying miRNA-mediated regulation of *sox10* expression and specific miRNAs during melanocyte vertebrate development.

5. Author contributions

AMJW and NBC contributed to conception, design of the experiments, and drafting of the manuscript. AMJW, NLS, and TJS performed the experiments, acquired the data, and analyzed the results. RNK revised the manuscript. CMD and EMB-N generated the mutant fish and revised the manuscript.

6. Acknowledgements

We are indebted to Sebastian Graziati and Marc Shedden for expert fish care. We thank Enrique Morales and Rodrigo Vena for help with microscope using and confocal imaging. This work was supported by an EMBO Short Term Fellowship (ASTF:370-2014 to AMJW), an ANPCyT PICT Grant (PICT-2014-1885 to NBC), a CONICET PIP Grant (PIP-2015-0719 to NBC), and a BBSRC grant (BB/L00769X/1 to RNK). NLS is a fellow, and AMJW and NBC are Staff Members of CONICET. TJS is a fellow of Consejo Interuniversitario Nacional 2017 (Becas Estímulo a las Vocaciones Científicas).

7. References

[1] W.P. Kloosterman, R.H.A. Plasterk, The Diverse Functions of MicroRNAs in Animal Development and Disease, Dev. Cell. 11 (2006) 441–450. doi:10.1016/j.devcel.2006.09.009.

[2] J.A. Vidigal, A. Ventura, The biological functions of miRNAs: Lessons from in vivo studies, Trends Cell Biol. 25 (2015) 137–147. doi:10.1016/j.tcb.2014.11.004.

[3] M.R. Fabian, N. Sonenberg, W. Filipowicz, Regulation of mRNA Translation and

Stability by microRNAs, Annu. Rev. Biochem. 79 (2010) 351–79. doi:10.1146/annurev-biochem-060308-103103.

[4] D.P. Bartel, MicroRNAs: Target Recognition and Regulatory Functions, Cell. 136 (2009) 215–233. doi:10.1016/j.cell.2009.01.002.

[5] E. Bernstein, S.Y. Kim, M.A. Carmell, E.P. Murchison, H. Alcorn, M.Z. Li, A.A. Mills, S.J. Elledge, K. V Anderson, G.J. Hannon, Dicer is essential for mouse development, Nat Genet. 35 (2003) 215–217. doi:10.1038/ng1253.

[6] E. Wienholds, M.J. Koudijs, F.J.M. van Eeden, E. Cuppen, R.H. a Plasterk, The microRNA-producing enzyme Dicer1 is essential for zebrafish development., Nat. Genet. 35 (2003) 217–8. doi:10.1038/ng1251.

[7] S. Akhtar, S.R. Patnaik, R. Kotapati Raghupathy, T.M. Al-Mubrad, J.A. Craft, X. Shu, Histological characterization of the Dicer1 mutant zebrafish retina, J. Ophthalmol. 2015 (2015) 1–9. doi:10.1155/2015/309510.

[8] A. Giraldez, R. Cinalli, M. Glasner, A. Enright, T. M;, B. S;, S. Hammond, D. Bartel, A. Schier, MicroRNAs Regulate Brain Morphogenesis in Zebrafish, Science. 308 (2005) 833–838. doi:10.1126/science.1109020.

[9] A.J. Giraldez, Y. Mishima, J. Rihel, R.J. Grocock, S. Van Dongen, K. Inoue, A.J. Enright, A.F. Schier, Zebrafish MiR-430 promotes deadenylation and clearance of maternal mRNAs, Science. 312 (2006) 75–79. doi:10.1126/science.1122689.

[10] A.A. Bazzini, M.T. Lee, A.J. Giraldez, Ribosome profiling shows that miR-430 reduces translation before causing mRNA decay in Zebrafish, Science. 336 (2012) 233–237. doi:10.1126/science.1215704.

[11] A.F. Schier, A.J. Giraldez, MicroRNA Function and Mechanism: Insights from Zebra Fish, Cold Spring Harb. Symp. Quant. Biol. LXXI (2006) 195–203.

doi:10.1101/sqb.2006.71.055.

[12] E. Theveneau, R. Mayor, Neural crest delamination and migration: From epithelium-to-mesenchyme transition to collective cell migration, Dev. Biol. 366 (2012) 34–54. doi:10.1016/j.ydbio.2011.12.041.

[13] E. Dupin, N.M. Le Douarin, The neural crest, A multifaceted structure of the vertebrates, Birth Defects Res. Part C - Embryo Today Rev. 102 (2014) 187–209. doi:10.1002/bdrc.21080.

[14] M.L. Martik, M.E. Bronner, Regulatory Logic Underlying Diversification of the Neural Crest, Trends Genet. 33 (2017) 715–727. doi:10.1016/j.tig.2017.07.015.

[15] A. Zehir, L.L. Hua, E.L. Maska, Y. Morikawa, P. Cserjesi, Dicer is required for survival of differentiating neural crest cells, Dev. Biol. 340 (2010) 459–467. doi:10.1016/j.ydbio.2010.01.039.

[16] X. Nie, Q. Wang, K. Jiao, Dicer activity in neural crest cells is essential for craniofacial organogenesis and pharyngeal arch artery morphogenesis, Mech. Dev. 128 (2011) 200–207. doi:10.1016/j.mod.2010.12.002.

[17] T. Huang, Y. Liu, M. Huang, X. Zhao, L. Cheng, Wnt1-cre-mediated conditional loss of Dicer results in malformation of the midbrain and cerebellum and failure of neural crest and dopaminergic differentiation in mice, J. Mol. Cell Biol. 2 (2010) 152–163. doi:10.1093/jmcb/mjq008.

[18] Z.P. Huang, J.F. Chen, J.N. Regan, C.T. Maguire, R.H. Tang, X. Rong Dong, M.W. Majesky, D.Z. Wang, Loss of MicroRNAs in neural crest leads to cardiovascular syndromes resembling human congenital heart defects, Arterioscler. Thromb. Vasc. Biol. 30 (2010) 2575–2586. doi:10.1161/ATVBAHA.110.213306.

[19] A.M.J. Weiner, MicroRNAs and the neural crest: From induction to

differentiation, Mech. Dev. (2018). doi:10.1016/j.mod.2018.05.009.

[20] P.H. Strobl-Mazzulla, M. Marini, A. Buzzi, Epigenetic landscape and miRNA involvement during neural crest development, Dev. Dyn. 241 (2012) 1849–1856. doi:10.1002/dvdy.23868.

[21] C.A. Hodgkinson, K.J. Moore, A. Nakayama, E. Steingrímsson, N.G. Copeland, N.A. Jenkins, H. Arnheiter, Mutations at the mouse microphthalmia locus are associated with defects in a gene encoding a novel basic-helix-loop-helix-zipper protein, Cell. 74 (1993) 395–404. doi:10.1016/0092-8674(93)90429-T.

[22] J.A. Lister, C.P. Robertson, T. Lepage, S.L. Johnson, D.W. Raible, nacre encodes a zebrafish microphthalmia-related protein that regulates neural-crest-derived pigment cell fate., Development. 126 (1999) 3757–3767.

[23] S. Goswami, R.S. Tarapore, A.M.P. Strong, J.J. TeSlaa, Y. Grinblat, V. Setaluri, V.S. Spiegelman, MicroRNA-340-mediated degradation of microphthalmia-associated transcription factor (MITF) mRNA is inhibited by coding region determinant-binding protein (CRD-BP), J. Biol. Chem. 290 (2015) 384–395. doi:10.1074/jbc.M114.590158.

[24] M.S. Stark, S. Tyagi, D.J. Nancarrow, G.M. Boyle, A.L. Cook, D.C. Whiteman, P.G. Parsons, C. Schmidt, R.A. Sturm, N.K. Hayward, Characterization of the melanoma miRNAome by deep sequencing, PLoS One. 5 (2010) e9685. doi:10.1371/journal.pone.0009685.

[25] C. Levy, M. Khaled, K.C. Robinson, R.A. Veguilla, P.H. Chen, S. Yokoyama, E. Makino, J. Lu, L. Larue, F. Beermann, L. Chin, M. Bosenberg, J.S. Song, D.E. Fisher, Lineage-specific transcriptional regulation of DICER by MITF in melanocytes, Cell. 141 (2010) 994–1005. doi:10.1016/j.cell.2010.05.004.

[26] R.E. Bell, C. Levy, The three M's: Melanoma, microphthalmia-associated transcription factor and microRNA, Pigment Cell Melanoma Res. (2011) 1088–1106. doi:10.1111/j.1755-148X.2011.00931.x.

[27] S. Elworthy, J. a Lister, T.J. Carney, D.W. Raible, R.N. Kelsh, Transcriptional regulation of mitfa accounts for the sox10 requirement in zebrafish melanophore development., Development. 130 (2003) 2809–2818. doi:10.1242/dev.00461.

[28] E.R. Greenhill, A. Rocco, L. Vibert, M. Nikaido, R.N. Kelsh, An iterative genetic and dynamical modelling approach identifies novel features of the gene regulatory network underlying melanocyte development, PLoS Genet. 7 (2011) e1002265. doi:10.1371/journal.pgen.1002265.

[29] M. Westerfield, The Zebrafish Book. A Guide for the Laboratory Use of Zebrafish (Danio rerio), 5th Edition, Univ. Oregon Press. Eugene. (2007).

[30] C.B. Kimmel, W.W. Ballard, S.R. Kimmel, Stages of embryonic development of the zebrafish, Dev. Dyn. 203 (1995) 253–310. doi:10.1002/aja.1002030302.

[31] W.J. Kent, BLAT — The BLAST -Like Alignment Tool, Genome Res. 12 (2002) 656–664. doi:10.1101/gr.229202.

[32] K.S. Solomon, Zebrafish foxi1 mediates otic placode formation and jaw development, Development. 130 (2003) 929–940. doi:10.1242/dev.00308.

[33] M.S. Porcel De Peralta, V.S. Mouguelar, M.A. Sdrigotti, F.A. Ishiy, R.D. Fanganiello, M.R. Passos-Bueno, G. Coux, N.B. Calcaterra, Cnbp ameliorates Treacher Collins Syndrome craniofacial anomalies through a pathway that involves redox-responsive genes, Cell Death Dis. 7 (2016) e2397. doi:10.1038/cddis.2016.299.

[34] D.R. Van Gijn, A.S. Tucker, M.T. Cobourne, Craniofacial development: Current concepts in the molecular basis of Treacher Collins syndrome, Br. J. Oral Maxillofac. Surg. 51 (2013) 384–388. doi:10.1016/j.bjoms.2012.09.008.

[35] C.A. Schneider, W.S. Rasband, K.W. Eliceiri, NIH Image to ImageJ : 25 years of image analysis, Nat. Methods. 9 (2012) 671–675. doi:10.1038/nmeth.2089.

[36] B. Fernandes, T. Matamá, D. Guimaraes, A. Gomes, A. Cavaco-Paulo, Fluorescent quantification of melanin, Pigment Cell Melanoma Res. (2016) 1–6. doi:10.1111/pcmr.12535.

[37] L. Fernandez Del Ama, M. Jones, P. Walker, A. Chapman, J.A. Braun, J. Mohr, A.F.L. Hurlstone, Reprofiling using a zebrafish melanoma model reveals drugs cooperating with targeted therapeutics, Oncotarget. 7 (2016) 40348–40361. doi:10.18632/oncotarget.9613.

[38] B.B. Kirby, N. Takada, A.J. Latimer, J. Shin, T.J. Carney, R.N. Kelsh, B. Appel, In vivo time-lapse imaging shows dynamic oligodendrocyte progenitor behavior during zebrafish development, Nat. Neurosci. 9 (2006) 1506–1511. doi:10.1038/nn1803.

[39] A.M.J. Weiner, M.A. Sdrigotti, R.N. Kelsh, N.B. Calcaterra, Deciphering the cellular and molecular roles of cellular nucleic acid binding protein during cranial neural crest development, Dev. Growth Differ. 53 (2011) 934–947. doi:10.1111/j.1440-169X.2011.01298.x.

[40] C. Thisse, B. Thisse, High-resolution in situ hybridization to whole-mount zebrafish embryos., Nat. Protoc. 3 (2008) 59–69. doi:10.1038/nprot.2007.514.

[41] R. Tang, A. Dodd, D. Lai, W.C. McNabb, D.R. Love, Validation of zebrafish (Danio rerio) reference genes for quantitative real-time RT-PCR normalization, Acta

Biochim. Biophys. Sin. (Shanghai). 39 (2007) 384–390. doi:10.1111/j.1745-7270.2007.00283.x.

[42] S.A. Bustin, V. Benes, J.A. Garson, J. Hellemans, J. Huggett, M. Kubista, R. Mueller, T. Nolan, M.W. Pfaffl, G.L. Shipley, J. Vandesompele, C.T. Wittwer, The MIQE Guidelines: Minimum Information for Publication of Quantitative Real-Time PCR Experiments, Clin. Chem. 55 (2009) 611–622. doi:10.1373/clinchem.2008.112797.

[43] C.M. Dooley, C. Scahill, F. Fényes, R.N.W. Kettleborough, D.L. Stemple, E.M. Busch-Nentwich, Multi-allelic phenotyping - A systematic approach for the simultaneous analysis of multiple induced mutations, Methods. 62 (2013) 197–206. doi:10.1016/j.ymeth.2013.04.013.

[44] R.N.W. Kettleborough, E.M. Busch-Nentwich, S.A. Harvey, C.M. Dooley, E. De Bruijn, F. Van Eeden, I. Sealy, R.J. White, C. Herd, I.J. Nijman, F. Fényes, S. Mehroke, C. Scahill, R. Gibbons, N. Wali, S. Carruthers, A. Hall, J. Yen, E. Cuppen, D.L. Stemple, A systematic genome-wide analysis of zebrafish protein-coding gene function, Nature. 496 (2013) 494–497. doi:10.1038/nature11992.

[45] Y. Li, J. Piatigorsky, Targeted deletion of dicer disrupts lens morphogenesis, corneal epithelium stratification, and whole eye development, Dev. Dyn. 238 (2009) 2388–2400. doi:10.1002/dvdy.22056.

[46] R.N. Kelsh, M. Brand, Y. Jiang, C. Heisenberg, S. Lin, P. Haffter, J. Odenthal, M.C. Mullins, F.J.M. Van Eeden, M. Furutani-seiki, M. Granato, M. Hammerschmidt, D.A. Kane, R.M. Warga, D. Beuchle, L. Vogelsang, C. Nüsslein-volhard, Zebrafish pigmentation mutations and the processes of neural crest development, Development. 123 (1996) 369–389.

[47] J.R. Dutton, A. Antonellis, T.J. Carney, F.S. Rodrigues, W.J. Pavan, A. Ward, R.N. Kelsh, BMC Developmental Biology An evolutionarily conserved intronic region controls the spatiotemporal expression of the transcription factor Sox10, BMC Dev. Biol. 8 (2008). doi:10.1186/1471-213X-8-105.

[48] Y. Cheli, M. Ohanna, R. Ballotti, C. Bertolotto, Fifteen-year quest for microphthalmia-associated transcription factor target genes, Pigment Cell Melanoma Res. (2010) 27–40. doi:10.1111/j.1755-148X.2009.00653.x.

[49] M. Lee, J. Goodall, C. Verastegui, R. Ballotti, C.R. Goding, Direct regulation of the microphthalmia promoter by Sox10 links Waardenburg-Shah syndrome (WS4)-associated hypopigmentation and deafness to WS2, J. Biol. Chem. 275 (2000) 37978–37983. doi:10.1074/jbc.M003816200.

[50] C. Verastegui, K. Bille, J.P. Ortonne, R. Ballotti, Regulation of the Microphthalmia-associated transcription factor gene by the Waardenburg syndrome type 4 gene, SOX10, J. Biol. Chem. 275 (2000) 30757–30760. doi:10.1074/jbc.C000445200.

[51] D. Bennett, Colour genes, oncogenes and melanocyte differentiation, J. Cell Sci. 98 (1991) 135–139.

[52] T. Kobayashi, W.D. Vieira, B. Potterf, C. Sakai, G. Imokawa, V.J. Hearing, Modulation of melanogenic protein expression during the switch from eu- to pheomelanogenesis., J. Cell Sci. 108 (Pt 6 (1995) 2301–2309.

[53] M.S. Marks, M.C. Seabra, The melanosome: Membrane dynamics in black and white, Nat. Rev. Mol. Cell Biol. 2 (2001) 738–748. doi:10.1038/35096009.

[54] H. Ozeki, S. Ito, K. Wakamatsu, T. Hirobe, Chemical characterization of hair melanins in various coat-color mutants of mice, J. Invest. Dermatol. 105 (1995)

361–366. doi:10.1111/1523-1747.ep12320792.

[55] K. Tsukamoto, A. Palumbo, M. D'Ischia, V.J. Hearing, G. Prota, 5,6-Dihydroxyindole-2-carboxylic acid is incorporated in mammalian melanin., Biochem. J. 286 (Pt 2) (1992) 491–5. doi:10.1042/bj2860491.

[56] E. Wienholds, W. Kloosterman, E. Miska, E. Alvarez-Saavedra, E. Berezikov, E. de Bruijn, R. Horvitz, S. Kauppinen, R. Plasterk, MicroRNA Expression in Zebrafish Embryonic Development, Science (80-.). 309 (2005) 310–311. doi:10.1126/science.1114519.

[57] X.H. Liang, S.T. Crooke, Depletion of key protein components of the RISC pathway impairs pre-ribosomal RNA processing, Nucleic Acids Res. 39 (2011) 4875–4889. doi:10.1093/nar/gkr076.

[58] L. Sinkkonen, T. Hugenschmidt, W. Filipowicz, P. Svoboda, Dicer is associated with Ribosomal DNA chromatin in mammalian cells, PLoS One. 5 (2010) 1–11. doi:10.1371/journal.pone.0012175.

[59] C. Varamo, M. Occelli, D. Vivenza, M. Merlano, C. Lo Nigro, MicroRNAs role as potential biomarkers and key regulators in melanoma, Genes Chromosom. Cancer. (2017) 3–10. doi:10.1002/gcc.22402.

[60] G. Van Rensburg, S. Mackedenski, C.H. Lee, Characterizing the coding region determinant-binding protein (CRD-BP)- Microphthalmia-associated transcription factor (MITF) mRNA interaction, PLoS One. 12 (2017) 1–18. doi:10.1371/journal.pone.0171196.

8. Figure legends

Figure 1. *Dicer1*^{sa9205} homozygous mutants display aberrant developmental phenotypes. **A:** Schematic of *dicer1* gene showing the point mutation site of *dicer1*^{sa9205} mutant; colored boxes identify the different motifs in wild-type Dicer1 protein. **B-I:** Representative images of live *dicer1*^{sa9205} homozygous mutant embryos and larvae (**D**, **E**, **G**, and **I**) and wild-type siblings (**B**, **C**, **F**, and **H**). Lateral views with head to the left, dorsal uppermost, of 28 (**B**-**D**), 32 (**C**-**E**), 48 (**F**-**G**), and 72 hpf (**H**-**I**) specimens. Insets show enlarged regions of the posterior brain (**B'**-**E'**) and yolk sac (**F'**-**I'**) in order to compare melanocyte differentiation phenotype. Blue (controls) and red (mutants) arches and ovals highlight the main differences observed between controls and mutants. In G and I, both blue and red marks are shown in order to compare phenotypic differences between controls and mutants. Black dashed lines in F, H, and I indicate different pictures of the same specimen token at different focus. Scale bars 250 µm in **E** for **B**-**E** and in **I** for **F**-**I**.

Figure 2: Dicer1 depletion adversely affects craniofacial cartilages development. (**A**) Bar graph showing the quantification, in arbitrary units (AU) and +S.E.M., of craniofacial parameters measured in control and *dicer1*^{sa9205} 4-dpf larvae (*$p<0.001$; two-tailed statistical *t*-test). Representative pictures over the graph illustrate the measurements taken. Meckel length: distance between Meckel cartilage and ceratohyal cartilages joint; Meckel area: area of the inner triangle defined by the Meckel cartilage; CH length: length of ceratohyal cartilage; PQ length: length of palatoquadrate+hyosymplectic cartilages; CH distance: distance between ceratohyal cartilages joint and lateral fins (white dashed line); Cranial distance: distance between the most anterior Meckel and lateral fins (white dashed line). (**B**) Bar graph showing

the quantification of Meckel and ceratohyal cartilage angles and +S.E.M. in control and *dicer1*^{sa9205} 4-dpf larvae (two-tailed statistical *t*-test, *p<0.001). Alcian Blue staining of head cartilages from control (**C**), *dicer1*^{sa9205} (**D**), and Dicer1-MO (**E**) 4 dpf larvae. All larvae in ventral views, cephalic to the left. Scale bar: 150 µm.

Figure 3. Dicer1 depletion affects NCC development. **A-F**: Incident light images of 3 dpf larvae showing eye and trunk iridophores (silver spots) in wild-type sibling (**A-B**), *dicer1*^{sa9205} mutant (**C-D**) and *dicer1*-morphants (**E-F**). Note decreased extent of iridophores on both eye and in lateral patches (white arrowhead) above the yolk sac. Pictures **A, C,** and **E**: lateral views while pictures **B, D,** and **F** dorsal views, head to the left. Scale bar 250 µm in **F** for **A-F. G-L**: Confocal fluorescent images of 38 (**G-J**), 43 (**H-K**), and 48 (**I-L**) hpf transgenic *sox10*:GFP embryos treated with Dicer1-mmMO (**G-I**) or Dicer1-MO (**J-L**) showing the posterior trunk. Transgenic embryos injected with Dicer1-MO displayed increased numbers of GFP-labeled cells; all lateral views, head to the left, dorsal uppermost. **M**: Graph showing the percentage of melanised pigment cells detectably expressing GFP at different stages (hpf) in Dicer1-mmMO (black line) or Dicer1-MO (dotted line) treated specimens (±S.E.M. n>5; two-tailed statistical *t*-test, *p*<0.001 for all stages except 33 hpf). The inset picture shows typical melanised cells as counted in the experiment, highlighting those detectably expressing GFP (black arrowhead) and those not expressing GFP (black arrow). **N**: Levels of melanin measured in Dicer1-mmMO (control), Dicer1-MO, and *dicer1*^{sa9205} mutant embryos at 28 and 48 hpf (+S.E.M., n=5). Statistically significant differences were found at 48 hpf (ANOVA, post-hoc Tukey test, ns: not significant, **p*<0.0001).

Figure 4. *Dicer1*-depleted embryos show reduced numbers of melanocytes. **A:** Number of melanocytes in a dorsal region of the head (indicated by a white triangle in the picture) in Dicer1-mmMO, *dicer1*-morphants and *dicer1*^{sa9205} mutants at 48 and 72 hpf. Statistically significant differences were found for all conditions (±S.E.M. n=3; ANOVA, **p*<0.0001; post-hoc Tukey test). **B:** Number of melanocytes in the lateral stripe of the posterior trunk (region limited with a black rectangle in the picture) in Dicer1-mmMO, *dicer1*-morphants and *dicer1*^{sa9205} mutants at 48 and 72 hpf. Statistically significant differences were found as indicated (±S.E.M. n=3; ANOVA, **p*<0.0001; post-hoc Tukey test). Scale bar 125 µm.

Figure 5. *Dicer1*-depleted embryos show increased cell death. **A:** Percentages of apoptotic classes of 28 hpf-staged embryos staining with Acridine Orange. Embryos were scored using a qualitative scale; representative images of embryos displaying low, medium, or high cell death (fluorescent signal in head and body) are shown on the right. The bar graph shows the distribution of each apoptotic class in Dicer1-mmMO/control embryos, *dicer1*-morphants, and *dicer1*^{sa9205} mutants. **B:** Relative levels of *bcl2l11* mRNA expression in Dicer1-mmMO/controls (black bars), compared to *dicer1*-morphants (light grey bars) or *dicer1*^{sa9205} (dark grey bars) embryos at 28, 32, and 36 hpf (+S.E.M., n=4). Statistically significant differences were found as indicated (ANOVA, post-hoc Tukey test, *p*-values in the graph). **C-L:** Pictures of Tg(*sox10*:mRFP) embryos injected with either Dicer1-mmMO (controls) or Dicer1-MO (morphants), stained with Acridine Orange and observed under Normarski (**C-L**) or confocal microscopy (**C'-L'**). Pictures **D** and **D'** show control embryos staged at 26 hpf. Pictures **E**, **E'**, and **E"** show *dicer1*-morphant embryos staged at 26 hpf. Pictures **G**, **G'**, **I**, **I'**, **K** and

K' show control embryos staged at 32 hpf. Pictures **H**, **H'**, **J**, **J'**, **L**, and **L'** show *dicer1*-morphant embryos staged at 32 hpf. The three different cranial NC streams are shown in **G'**, **H'**, **I'**, and **J'**. Black segmented rectangles in **C** and **F** delimit the embryonic regions observed in **D'**-**E'**-**E"**, and for **G'**-**J'**, respectively. White arrowheads in **E'**, **E"**, **H'**, and **J'** highlight a subset of green or yellow apoptotic nuclei of NCC. All lateral views with dorsal up and eye to the left. o, otic vesicle; y, yolk. Scale bars 125 μm.

Figure 6. The depletion of Mitfa affects *dicer1* expression. **A**: Representation of the region of zebrafish *dicer1* gene spanning -3000 bp upstream the Transcription Start Site (+1) and the first exon sequences. Twelve putative binding sites for Mitfa (E-box: CANNTG) are highlighted with yellow circles and the single E-box conserved in zebrafish, mouse, and human *Dicer* promoters is marked with an orange circle (CATGTG). **B**: Relative amount of *dicer1* mRNA in *mitfa*$^{w2/w2}$ mutants (grey bars) normalized against the amount measured in wild type AB controls (black bars) at different stages during melanocyte development (+S.E.M., n=4). Statistically significance differences were obtained in *mitfa*$^{w2/w2}$ mutants at 30 and 36 hpf (two-tailed statistical *t*-test, *p*-values in the graph).

Figure 7. *Dicer1*-depleted embryos show increased levels of *sox10* and *mitfa* mRNAs. **A-B:** Relative levels of mRNA amount of *sox10* (**A**) and *mitfa* (**B**) genes in Dicer1-mmMO (control), Dicer1-MO, and *dicer1*^{sa9205} mutants; bars represent values measured at each developmental stage normalized to the amount of the corresponding mRNA measured in controls at 28, 32, 36, and 48 hpf (+S.E.M., n=4; ANOVA, post-hoc Tukey test, significance differences and *p*-values in the graph).

Whole mount *in situ* hybridization of *sox10* (**C**-**H**) and *mitfa* (**I**-**N**) genes in controls (**C**, **E**, **G**, **I**, **K**, and **M**) and *dicer1*^{sa9205} mutants (**D**, **F**, **H**, **J**, **L**, and **N**) at 28 (**C**-**D** and **I**-**J**), 32 (**E**-**F** and **K**-**L**), and 40 (**G**-**H** and **M**-**N**) hpf. White ovals and boxes highlight the main differences detected in *sox10* gene expression pattern. All pictures: lateral views, head to the left, dorsal uppermost. Scale bar: 250 µm. **O-Q:** Relative levels of mRNA amount of *dct* (**A**), *tyr* (**B**), and *tyrp1b* (**C**) genes in Dicer1-mmMO (control), Dicer1-MO, and *dicer1*^{sa9205} mutants; bars represent values measured at each developmental stage normalized to the amount of the corresponding mRNA measured in controls at 28, 32, 36, and 48 hpf (+S.E.M., n=4; ANOVA, post-hoc Tukey test, significance differences and *p*-values in the graph).

Figure 8. *sox10* and *mitfa* 3'UTRs affect the expression of EGFP reporter**. A**: Results from sequence analysis of *sox10*-3'UTR by Targetscan program. Conserved binding sites for putative miRNAs are highlighted with violet (an exact match to positions 2-8 of the mature miRNA, followed by an "A"), red (an exact match to positions 2-8 of the mature miRNA), and light blue (an exact match to positions 2-7 of the mature miRNA, followed by an "A") rectangles with the name of each miRNA family. Fragments F0, F1, and F2 for *sox10*-3'UTR are denoted with a yellow line. **B**: Results from sequence analysis of *mitfa*-3'UTR by Targetscan program. Conserved sites for putative miRNA are highlighted behind the blue line with violet, red, and light blue rectangles with the name of each miRNA family, as described above. **C:** Schematic representation of the experimental strategy followed for the study of EGFP expression. **D:** *Top* - Western blot showing the levels of EGFP in embryos at 24 hpf injected with SV40-poly(A), *sox10*-3'UTR, and *mitfa*-3'UTR samples. *Bottom* - Relative EGFP levels normalized to levels of

actin (+S.E.M., n=3; two-tailed statistical *t*-test, significance differences and *p*-values in the graph). **E**: Relative *EGFP* mRNA levels measured in 24 and 30 hpf staged embryos injected with SV40-poly(A), *sox10*-3'UTR, or *mitfa*-3'UTR (+S.E.M., n=4; two-tailed statistical *t*-test, significance differences and *p*-values in the graph). **F:** Relative *EGFP* mRNA levels in embryos of 24 hpf injected with SV40-poly(A), *sox10*-3'UTR, or *mitfa*-3'UTR mRNAs and with either Dicer1-mmMO (black bars) or Dicer1-MO (light grey bars) (+S.E.M., n=4; two-tailed statistical *t*-test, significance differences and *p*-values in the graph). **G:** Relative *EGFP* mRNA levels in 24 hpf embryos injected with F0-*sox10*-3'UTR, F1-*sox10*-3'UTR, or F2-*sox10*-3'UTR mRNAs and with either Dicer1-mmMO (black bars) or Dicer1-MO (light grey bars) (+S.E.M., n=4; two-tailed statistical *t*-test, significance differences and *p*-values in the graph). **H**: Melanocyte GRN suggested based on results gathered in this study and adapted from Greenhill et al., 2011. In red are highlighted the suggested new members and interactions resulted from this work. Complete lines show direct interactions and dotted lines probable direct/indirect interactions.

Supplementary Figure 1. Complementary information for *dicer1*^{sa9205} mutant. **A:** Results from different crosses between wild types and *dicer1*^{sa9205} mutant adults. **B:** Graph showing DNA sequence obtained from *wild type*, *dicer1*^{sa9205} heterozygote, and *dicer1*^{sa9205} homozygote embryo genotyping.

Supplementary Figure 2. Comparison of Dicer1-MO and Dicer1-mmMO phenotypes during development. **A-H:** Pictures of live embryos and larvae of Dicer1-mmMO control (**A**, **C**, **E**, and **G**) and *dicer1*-morphant (**B**, **D**, **F**, and **H**) phenotypes. Lateral views

with cephalic to the left and dorsal uppermost of 26 (**A**-**B**), 32 (**C**-**D**), 48 (**E**-**F**), and 72 hpf (**G**-**H**) specimens. Insets in **E-H** show enlarged regions of the yolk sac showing melanocyte differentiation phenotype. Scale bar 250 µm in **A** for **A**-**B**, in **D** for **C**-**D,** and in **H** for **E**-**H**.

Supplementary Figure 3. Dicer1-depletion affects *tyr* mRNA expression. Whole mount *in situ* hybridization of *dct* (**A**-**F**), *tyr* (**G**-**L**), and *tyrp1b* (**M**-**R**) genes in controls (**A**, **C**, **E**, **G**, **I**, **K**, **M**, **O**, and **Q**) and *dicer1*^{sa9205} mutants (**B**, **D**, **F**, **H**, **J**, **L**, **N**, **P**, and **R**) at 28 (**A**-**B**, **G**-**H**, and **M**-**N**), 32 (**C**-**D**, **I**-**J**, and **O**-**P**), and 40 (**E**-**F**, **K**-**L**, and **Q**-**R**) hpf. All pictures: lateral views, head to the left, dorsal uppermost. Scale bars: 250 µm in **F** for **A**-**F** and **M**-**R**; and in **L** for **G**-**L**.

Conflict of interest
The authors have declared that no conflict of interest exists.

Highlights

Dicer1-depleted zebrafish embryos showed improper black pigment cell pattern as well as defects in other neural crest derivatives.

Dicer1-depleted zebrafish phenotype is probably due to the apoptosis of neural crest cells.

Dicer1 and miRNAs are involved in the regulation of *sox10* and *mitfa* expression during melanocyte differentiation.

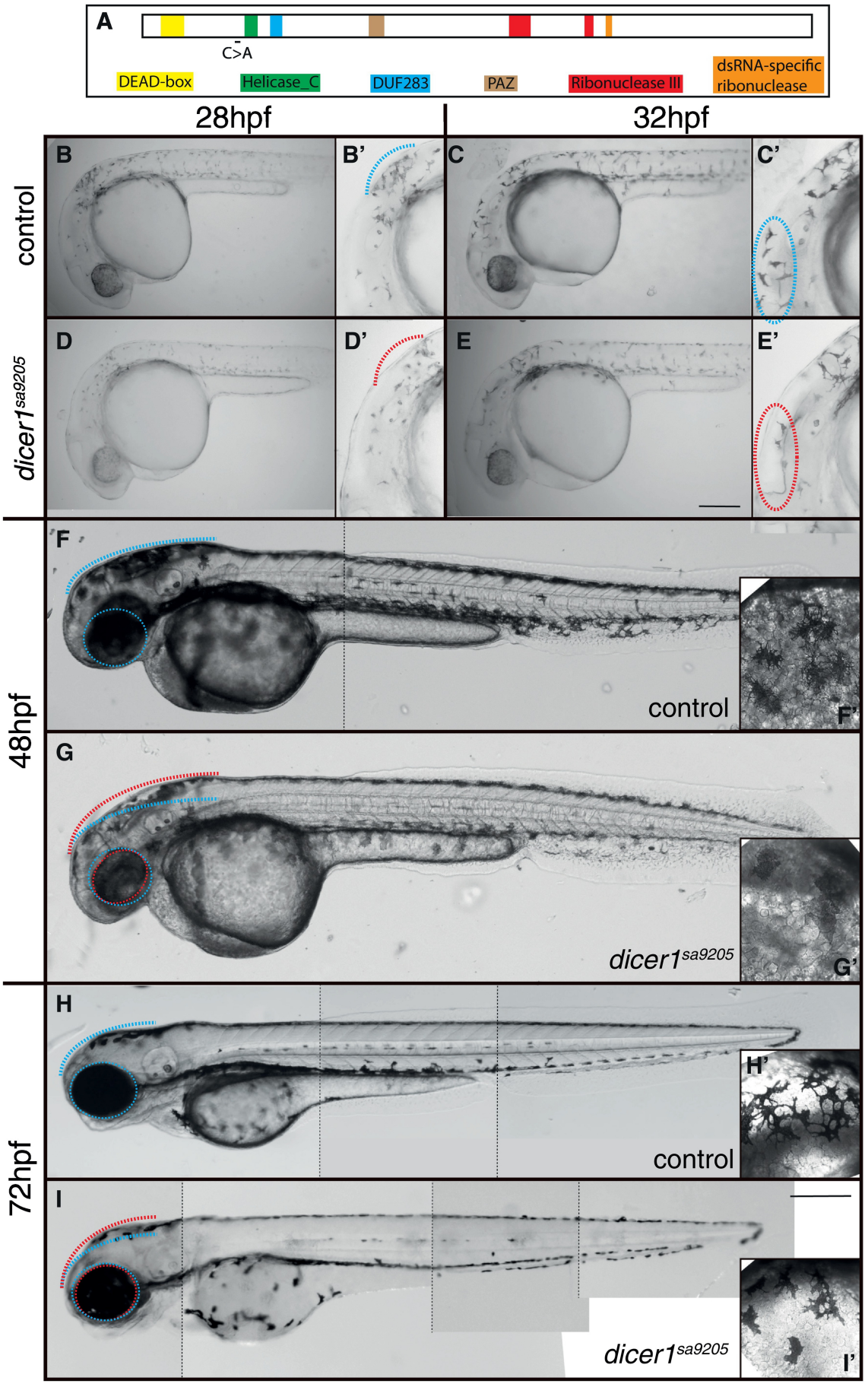
A
C>A
DEAD-box
Helicase_C
DUF283
PAZ
Ribonuclease III
dsRNA-specific ribonuclease
28hpf
32hpf
control
dicer1sa9205
B
B'
C
C'
D
D'
E
E'
48hpf
F
F'
control
G
G'
dicer1sa9205
72hpf
H
H'
control
I
I'
dicer1sa9205

Figure 1

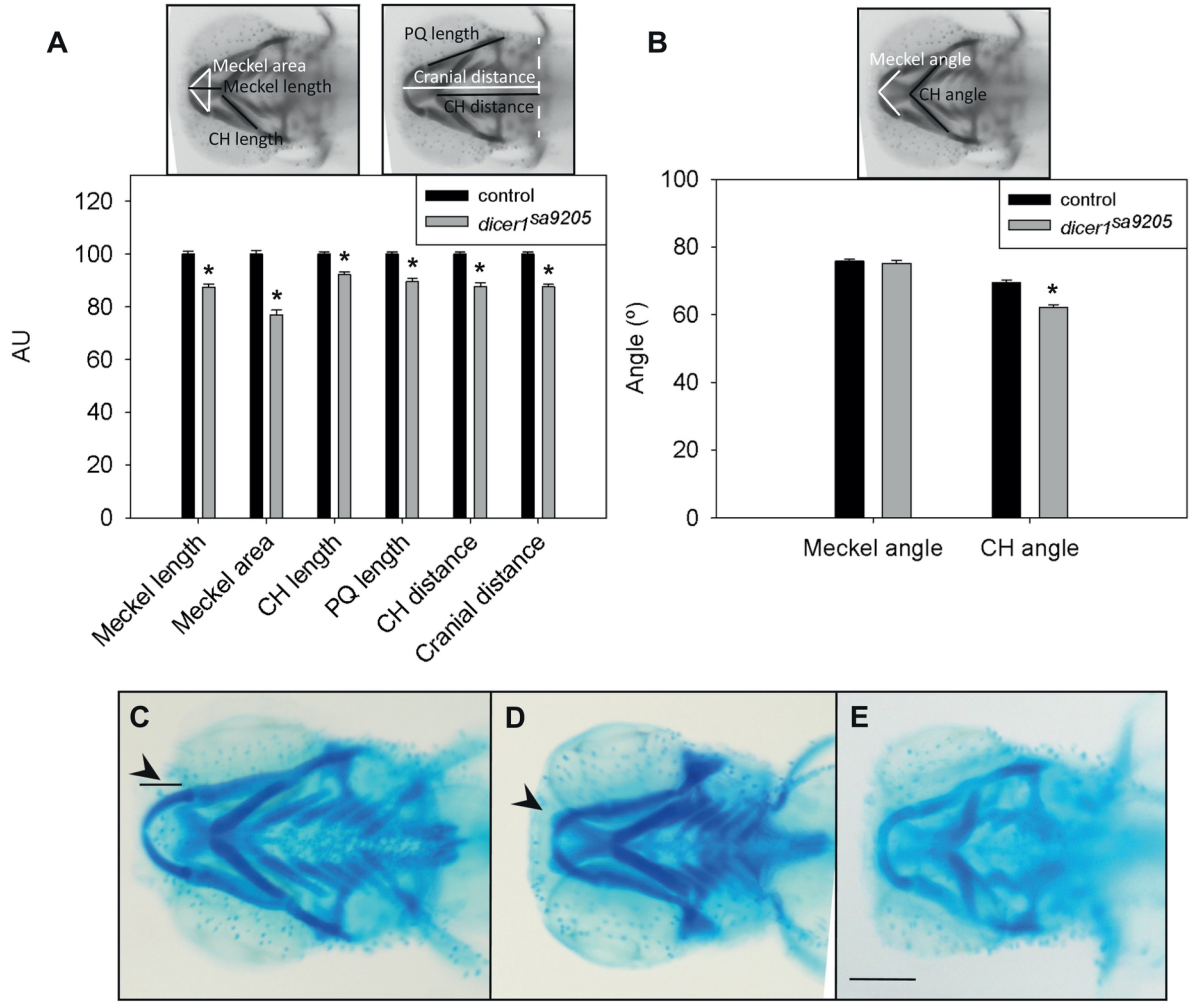
A
Meckel area
Meckel length
CH length
PQ length
Cranial distance
CH distance
control
dicer1sa9205
AU
120
100
80
60
40
20
0
Meckel length
Meckel area
CH length
PQ length
CH distance
Cranial distance
B
Meckel angle
CH angle
Angle (°)
100
80
60
40
20
0
Meckel angle
CH angle
C
D
E

Figure 2

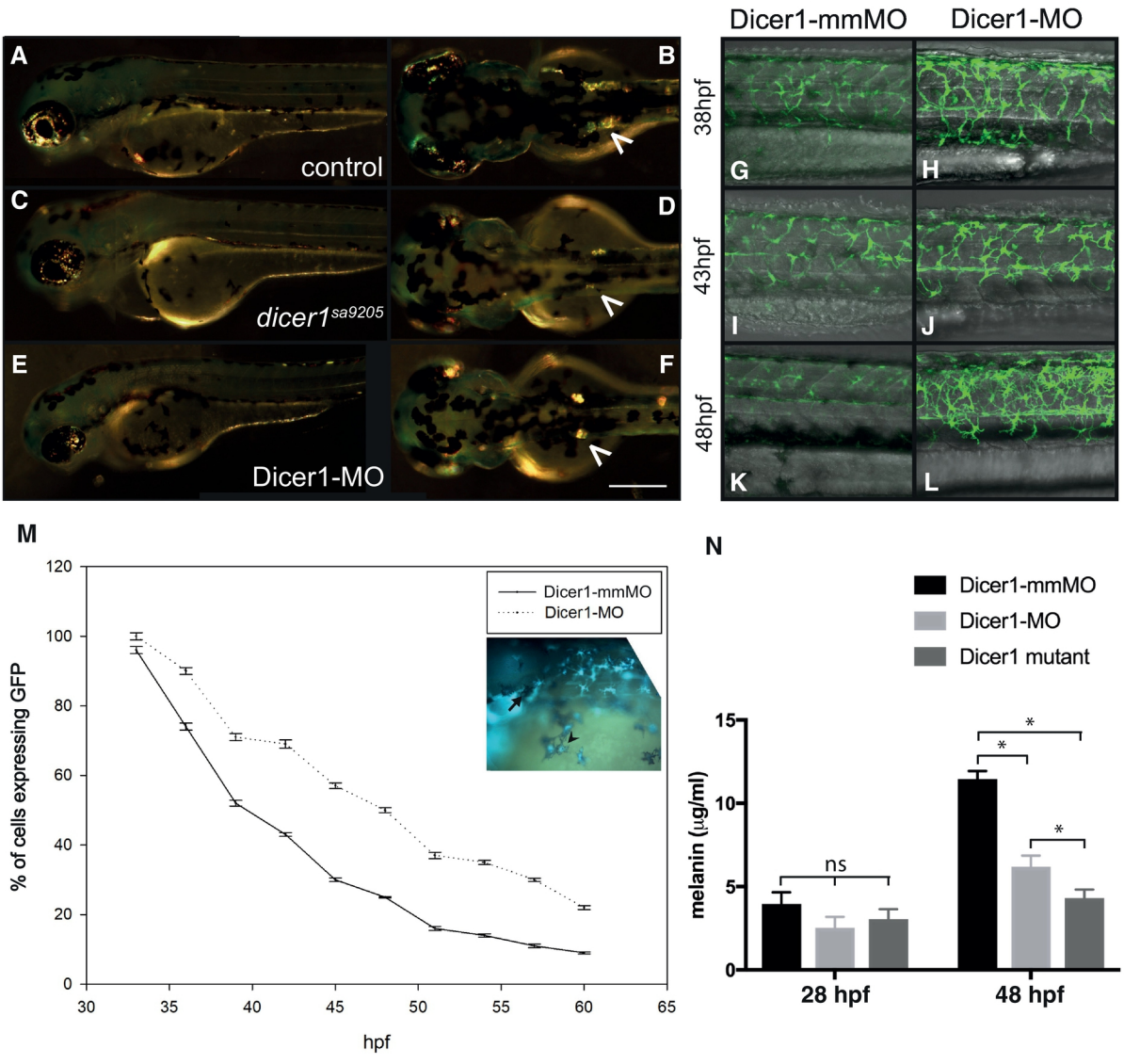
A
B
control
C
D
dicer1sa9205
E
F
Dicer1-MO
Dicer1-mmMO
Dicer1-MO
38hpf
43hpf
48hpf
G
H
I
J
K
L
M
% of cells expressing GFP
hpf
Dicer1-mmMO
Dicer1-MO
N
melanin (µg/ml)
Dicer1-mmMO
Dicer1-MO
Dicer1 mutant
ns
*
28 hpf
48 hpf

Figure 3

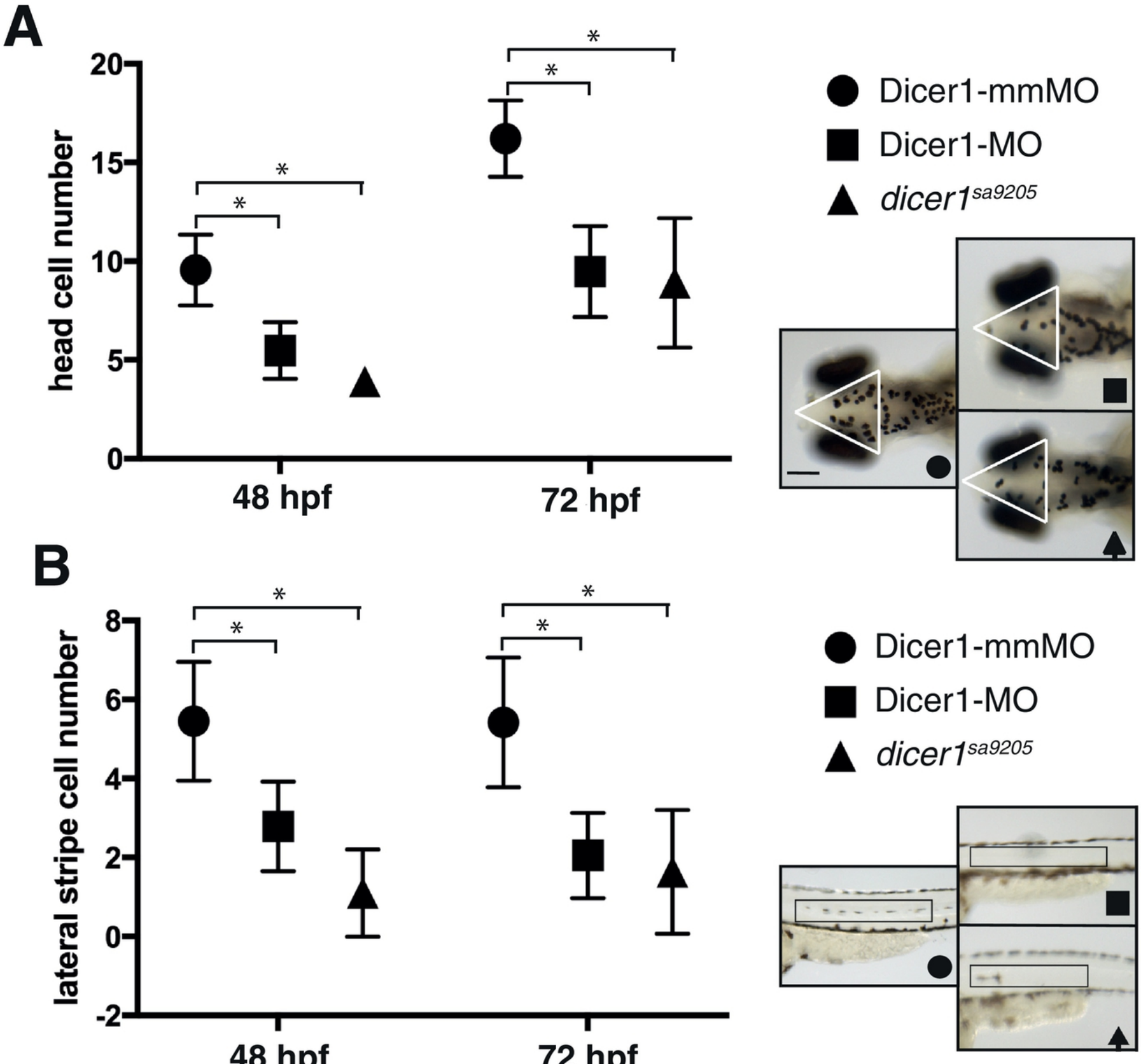
A
head cell number
20
15
10
5
0
48 hpf
72 hpf
*
*
*
*
Dicer1-mmMO
Dicer1-MO
dicer1sa9205
B
lateral stripe cell number
8
6
4
2
0
-2
48 hpf
72 hpf
*
*
*
*
Dicer1-mmMO
Dicer1-MO
dicer1sa9205

Figure 4

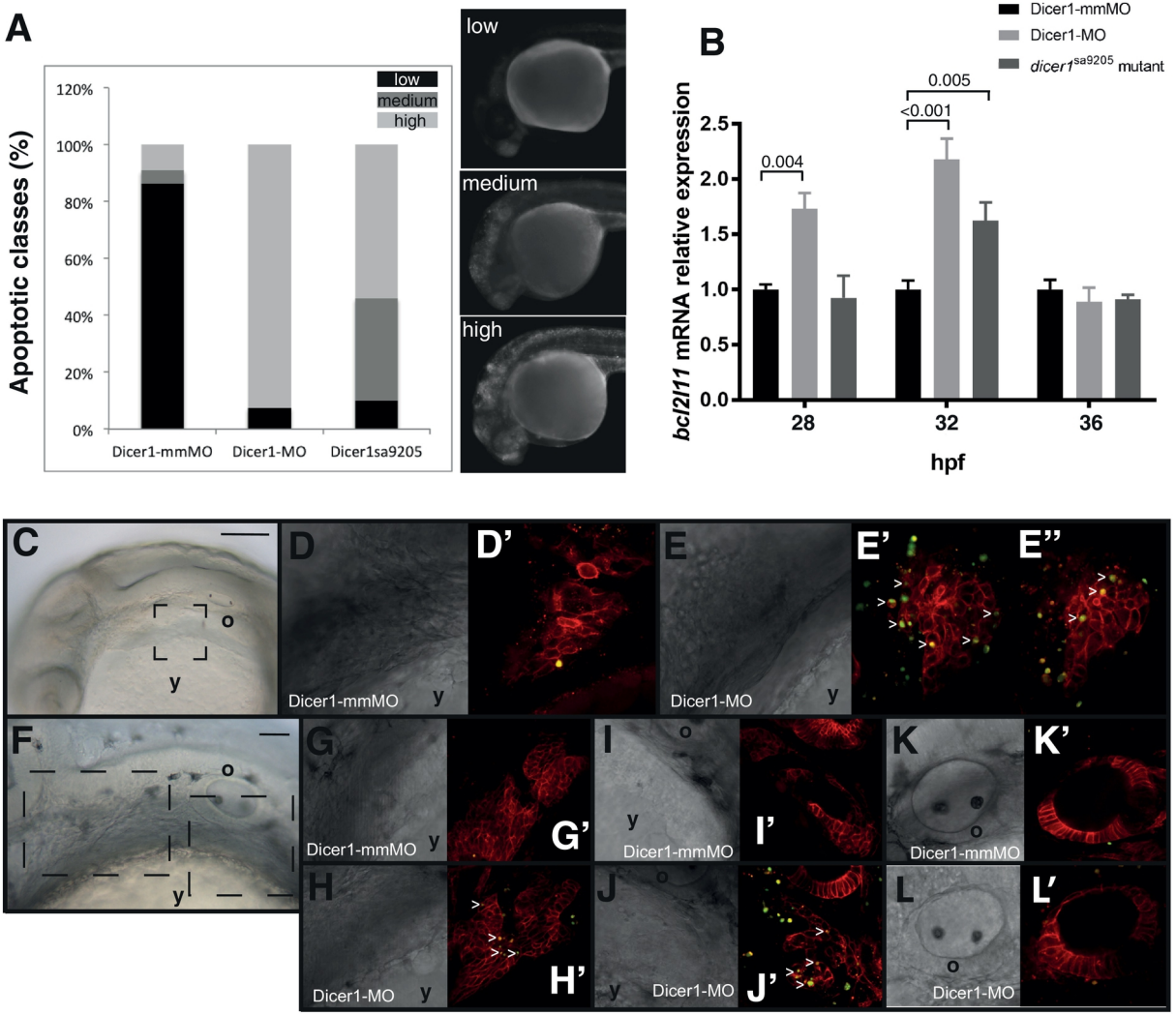
A
Apoptotic classes (%)
120%
100%
80%
60%
40%
20%
0%
low
medium
high
Dicer1-mmMO
Dicer1-MO
Dicer1sa9205
low
medium
high
B
Dicer1-mmMO
Dicer1-MO
dicer1sa9205 mutant
bcl2l11 mRNA relative expression
2.5
2.0
1.5
1.0
0.5
0.0
0.004
0.005
<0.001
28
32
36
hpf
C
D
D'
E
E'
E''
F
G
G'
I
I'
K
K'
H
H'
J
J'
L
L'
o
y
Dicer1-mmMO
Dicer1-MO

Figure 5

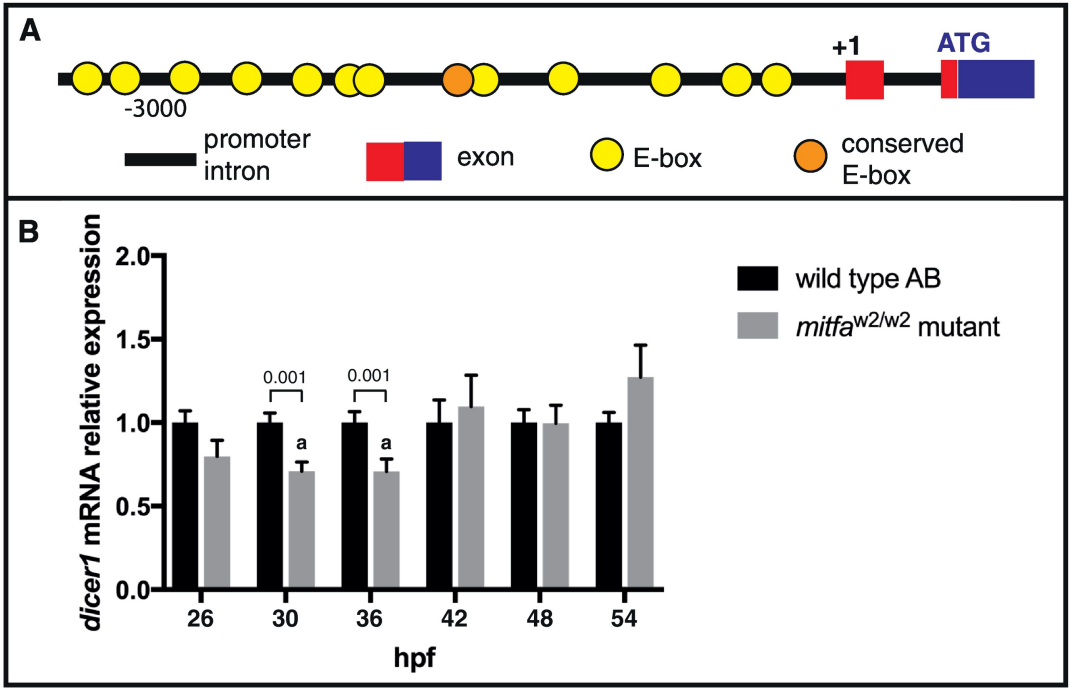
A
+1
ATG
-3000
promoter
intron
exon
E-box
conserved
E-box
B
dicer1 mRNA relative expression
2.0
1.5
1.0
0.5
0.0
0.001
0.001
a
a
26
30
36
42
48
54
hpf
wild type AB
mitfaw2/w2 mutant

Figure 6

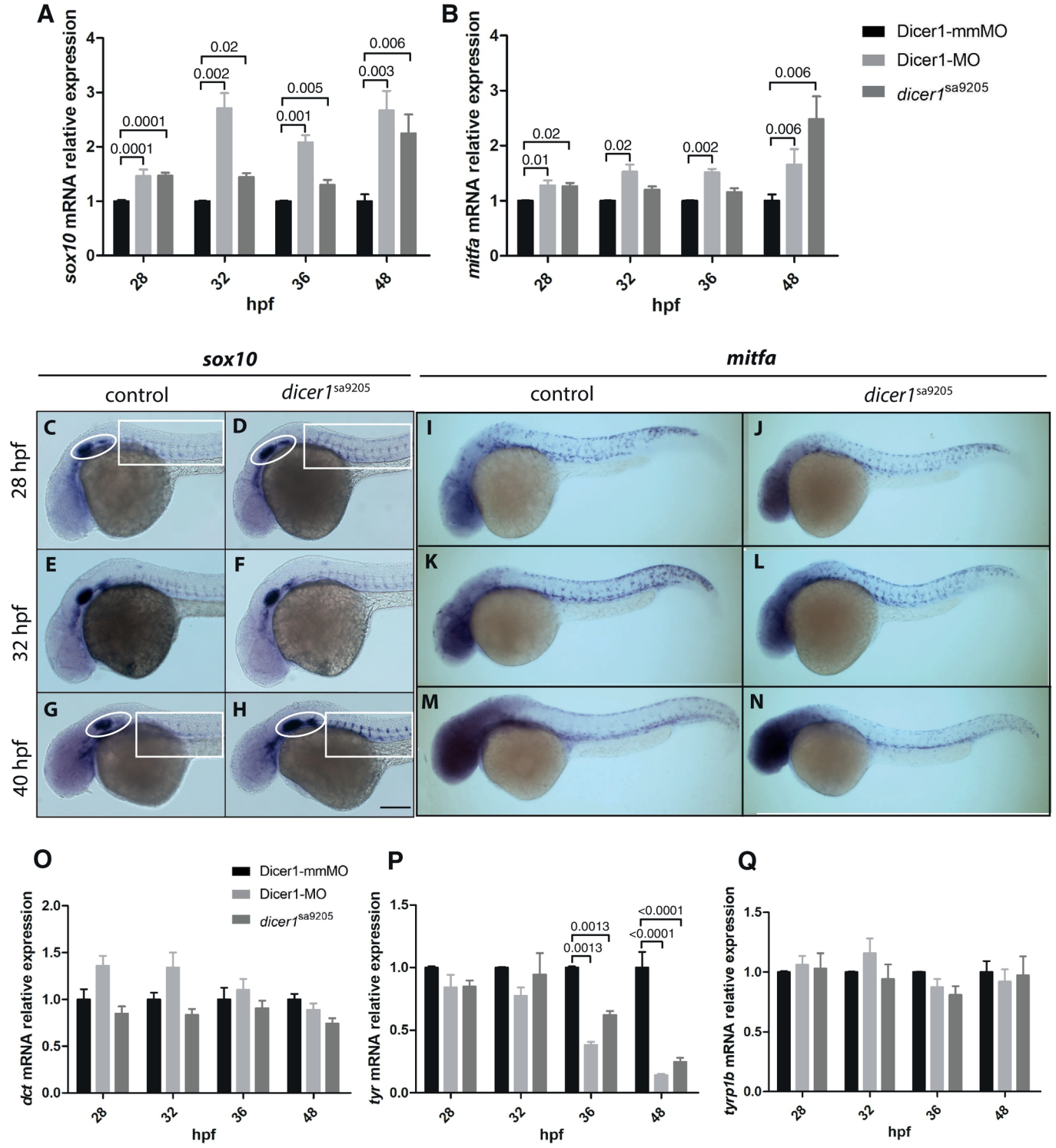
A
sox10 mRNA relative expression
0.0001
0.0001
0.002
0.02
0.001
0.005
0.003
0.006
28
32
36
48
hpf
B
mitfa mRNA relative expression
0.01
0.02
0.02
0.002
0.006
0.006
Dicer1-mmMO
Dicer1-MO
dicer1sa9205
sox10
mitfa
control
dicer1sa9205
28 hpf
32 hpf
40 hpf
C
D
E
F
G
H
I
J
K
L
M
N
O
dct mRNA relative expression
P
tyr mRNA relative expression
0.0013
0.0013
<0.0001
<0.0001
Q
tyrp1b mRNA relative expression

Figure 7

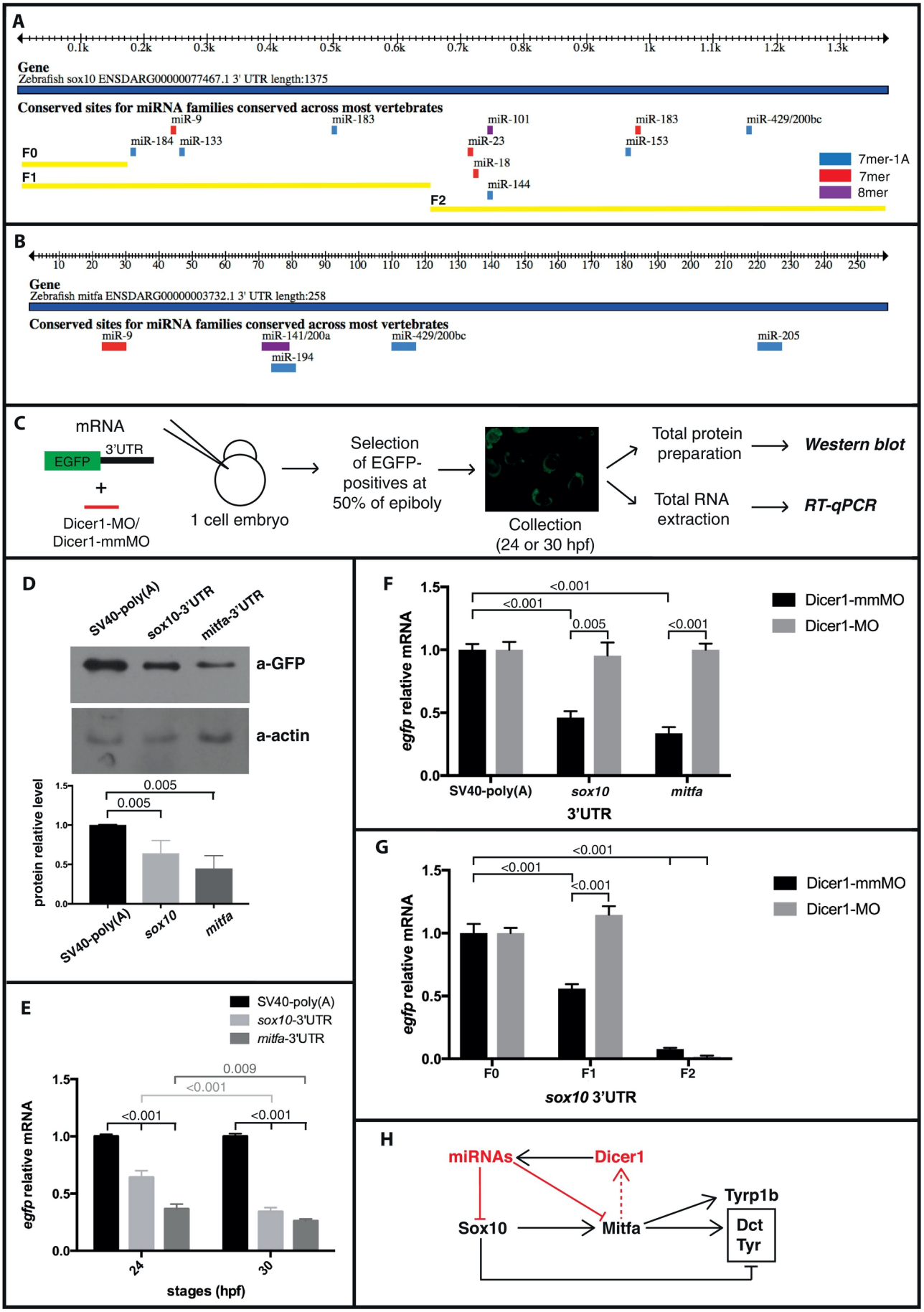
A
Gene
Zebrafish sox10 ENSDARG00000077467.1 3' UTR length:1375
Conserved sites for miRNA families conserved across most vertebrates
miR-9
miR-183
miR-101
miR-183
miR-429/200bc
miR-184
miR-133
miR-23
miR-153
miR-18
miR-144
F0
F1
F2
7mer-1A
7mer
8mer
B
Gene
Zebrafish mitfa ENSDARG00000003732.1 3' UTR length:258
Conserved sites for miRNA families conserved across most vertebrates
miR-9
miR-141/200a
miR-429/200bc
miR-205
miR-194
C
mRNA
EGFP
3'UTR
+
Dicer1-MO/
Dicer1-mmMO
1 cell embryo
Selection of EGFP-positives at 50% of epiboly
Collection (24 or 30 hpf)
Total protein preparation
Western blot
Total RNA extraction
RT-qPCR
D
SV40-poly(A)
sox10-3'UTR
mitfa-3'UTR
a-GFP
a-actin
protein relative level
0.005
0.005
SV40-poly(A)
sox10
mitfa
E
SV40-poly(A)
sox10-3'UTR
mitfa-3'UTR
egfp relative mRNA
0.009
<0.001
<0.001
<0.001
24
30
stages (hpf)
F
egfp relative mRNA
<0.001
<0.001
0.005
<0.001
Dicer1-mmMO
Dicer1-MO
SV40-poly(A)
sox10
mitfa
3'UTR
G
egfp relative mRNA
<0.001
<0.001
<0.001
Dicer1-mmMO
Dicer1-MO
F0
F1
F2
sox10 3'UTR
H
miRNAs
Dicer1
Sox10
Mitfa
Tyrp1b
Dct
Tyr

Figure 8